Acta Pharmaceutica Sinica B 2026;16(1):423−443

Chinese Pharmaceutical Association
Institute of Materia Medica, Chinese Academy of Medical Sciences

Acta Pharmaceutica Sinica B

www.elsevier.com/locate/apsb
www.sciencedirect.com

ORIGINAL ARTICLE

Dual metabolic-inflammation modulation in MicroRNA@neutrophil-derived microvesicles achieve robust osteoarthritis therapy

Yijun Chen, Yongbin Wang, Ruonan Yan, Yichen Liu, Yupeng Dai, Lingjing Xue, Caoyun Ju*, Can Zhang*

State Key Laboratory of Natural Medicines, Jiangsu Key Laboratory of Drug Discovery for Metabolic Diseases, Center of Advanced Pharmaceuticals and Biomaterials, China Pharmaceutical University, Nanjing 211198, China

Received 21 May 2025; received in revised form 31 July 2025; accepted 25 August 2025

KEY WORDS

Microvesicles;
Neutrophils;
MicroRNA;
Osteoarthritis;
Synergistic effect;
Cartilage penetration;
Anti-inflammation;
Metabolic homeostasis

Abstract Osteoarthritis (OA) presents significant therapeutic challenges due to the irreversible cartilage loss driven by chondrocyte metabolic imbalance and a severe inflammatory microenvironment. Conventional treatments are limited by poor chondrocyte-targeting and ineffectiveness of single-target medication. Here, we develop an anti-inflammatory neutrophil-derived microvesicle (MV)-based gene therapy for OA treatment, which leverages the intrinsic cartilage-penetrating capabilities of MVs to improve the targeted delivery of microRNA-140-5p (miR140) to chondrocytes, and the synergistic effect of anti-inflammatory MVs and miR140 to dual modulate the metabolic homeostasis of chondrocytes and the inflamed microenvironment. We demonstrate that miR140@MVs not only alleviate synovial inflammation *via* reprogramming the phenotypes of macrophages and adsorbing inflammatory factors, but also restore normal cartilage thickness in a destabilized medial meniscus mouse model due to the rebuilt metabolic homeostasis of chondrocytes, thus gaining a remarkable therapeutic effect up to 28 days. This study provides an immuno-stimulation method for production of anti-inflammatory MVs, and puts forward a safe and effective MVs-based miRNA system for treatment of joint-related diseases.

*Corresponding authors.
E-mail addresses: zhangcan@cpu.edu.cn (Can Zhang), jucaoyun@cpu.edu.cn (Caoyun Ju).

Peer review under the responsibility of Chinese Pharmaceutical Association and Institute of Materia Medica, Chinese Academy of Medical Sciences.

https://doi.org/10.1016/j.apsb.2025.09.020

1. Introduction

Osteoarthritis (OA) is a highly prevalent degenerative joint disease that might lead to permanent disability, affecting approximately 7% of the global population[1]. Especially, there will be more affected patients with the increase of the aging population[2,3]. Despite this significant medical need, no current treatment can halt OA progression; available therapies only alleviate pain and inflammation[4,5]. The primary challenge for OA is mainly ascribed to the irreversible cartilage damage mediated or exacerbated by metabolic imbalance in chondrocytes[6–9]. Chondrocytes, the sole cell type sparsely distributed throughout articular cartilage, serve as the producers of extracellular matrix (ECM), which is basically composed of type II collagen (COL II) and aggrecans. As OA progresses, chondrocytes senesce and die gradually[10], leading to insufficient ECM production. Meanwhile, the levels of two main enzymes responsible for ECM degradation including matrix metalloproteinase-13 (MMP-13)[11,12] and a disintegrin and metalloproteinase with thrombospondin motifs (ADAMTS-5)[2,13,14] increase by the production of senesced chondrocytes. Since the increased enzymatic degradation and the deficient formation of ECM, damaged cartilage results in further degeneration. The accompanying serious synovial inflammation in turn produces additional pro-inflammatory and catabolic products to further deteriorate the chondrocytes[2]. Due to the feedback-loop of OA progression, common medications such as anti-inflammatory small molecules[15], cytokine receptor antagonists[16], anabolic growth factors[17], and targeted inhibitors of catabolic enzymes[5], display unsatisfactory effectiveness. Therefore, breaking the feedback-loop of OA progression and restoring the metabolic homeostasis of chondrocytes shows promise in arresting and even reversing cartilage breakdown.

Differing from single-target medication, microRNA (miRNA) has the potential to take effect *via* modulating multiple genes[18]. Of which, miRNA-140-5p (hereafter referred to miR140) serves as the critical cartilage-specific miRNA[19], whose level reduces significantly in OA-impaired cartilage than that of healthy persons[20]. In special, miR140 can modulate senesced chondrocytes through suppressing genes such as *MMP13*[21], *ADAMTS5*[22], and *FUT1*[23] mRNA to inhibit ECM degradation and promote collagen biosynthesis. Also, miR140 can inhibit the expression of *TLR4*[24] and *TRAF6*[24] mRNA in macrophages to attenuate inflammatory cascades. Thus, complementing miR140 into impaired cartilage would make sense, yet without an effective therapy effect till now. The rapid clearance from the joint space (*e.g.*, the half-life is only 2−4 h)[25,26] and the liable degradation of miRNA lead to insufficient retention in the joint[27]. Moreover, the specific cartilage structure featuring dense (with pores of only 60 nm)[28], anionic and avascular tissue, intensifies the difficulty of miRNA entering chondrocytes dispersed in cartilage. Recently, lipid nanoparticles (LNPs) which can effectively encapsulate mRNA and antibody have emerged as promising vehicles for intra-articular drug delivery with deep penetration, thus exhibiting robust protection against osteoarthritis[29]. While the retention of nanocarriers in cartilage remains a challenge. To this end, small cationic nanocarriers (<15 nm) have been developed to improve the retention of miRNA owing to their small size and positive charge to adhere to the negative ECM[30,31]. However, the dilemma of free movement of cationic nanocarriers in dense and anionic cartilage tissue restricts their entrance into chondrocytes[28,30,31].

Extracellular vesicles, which have good biocompatibility and a natural tendency to a specific site, show promise in intra-articular drug delivery. Notably, neutrophil-derived microvesicles (MVs), a kind of endogenous extracellular vesicles generated by budding from neutrophils, have been evidenced to be the most abundant extracellular vesicles in the inflammatory synovial fluid[32] and can be found in the dense cartilage[33], suggesting their robust potential of being the miRNA carriers due to the effective cartilage infiltration. More beneficially, MVs inherit the membrane proteins of neutrophils, such as Annexin A1 (Anx A1) and other inflammatory factor receptors, implying the anti-inflammatory capability, rather than the pro-inflammatory effect of exosomes derived from neutrophils[32]. However, when the anti-inflammatory capacity of MVs is insufficient, long-term MV treatment may lead to oxidative damage in synovial fibroblasts[34] and inflammation in endothelial cells[35], which is detrimental to the management of osteoarthritis.

Herein, we propose to leverage the autonomous cartilage-penetrating capability of MVs to deliver miR140 for prolonged OA treatment (Fig. 1). To further improve MVs with sufficient anti-inflammatory effect, we would upgrade the production method of MVs *via* immune-stimulation on neutrophils first. The proteomic analysis of upgraded MVs was explored to evaluate the effectiveness of this production method. Based on this, we further fabricated a synergized MV system (miR140@MVs) encapsulating miR140 *via* electroporation. After intra-articular injection into the destabilized medial meniscus (DMM) mouse model, miR140@MVs could autonomously transport across the dense cartilage matrix and reach the chondrocytes deep in the impaired cartilage, where they effectively delivered the encapsulated miR140 to the endoplasmic reticulum (ER) of chondrocytes to multiply regulate the metabolic homeostasis of senescent chondrocytes. Meanwhile, miR140@MVs could remodel the inflamed microenvironment of OA by converting macrophages from M1 phenotypes towards M2 ones and neutralizing the inflammatory factors, thus avoiding OA deterioration. We believe that this simple and multifunctional MV system holds the prospects for clinical OA treatment.

2. Materials and methods

2.1. Ethics statement

All animal experimental protocols were approved by the Animal Experimentation Ethics Committee of China Pharmaceutical University (2024-11-049). The animals were kept in the specific pathogen free (SPF) barrier facilities. The cervical dislocation was used to confirm the death of experimental animals.

2.2. Materials

MiR140, Cy3-miR140 and Cy5-miR140 were purchased from RiboBio Tech (Guangzhou, China). For cell culture, DMEM, RPMI, PBS and penicillin−streptomycin were purchased from Hyclone (Logan, UT, USA), and fetal bovine serum (FBS) was bought from Gibco (Grand Island, NY, USA). IL1β and TNFα were bought from Peprotech (NJ, USA). LPS was purchased from Sigma−Aldrich. Apoptosis Detection Kit and q-PCR related agents, including RNA isolater Total RNA Extraction Reagent, HiScript III 1st Strand cDNA Synthesis Kitwere and AceQ qPCR SYBR Green Master Mix were bought from Vazyme (Nanjing, China). Anti-ADAMTS5 antibody (abs116232), anti-Collagen II antibody (abs13155) and anti-GAPDH antibody (abs132004) were

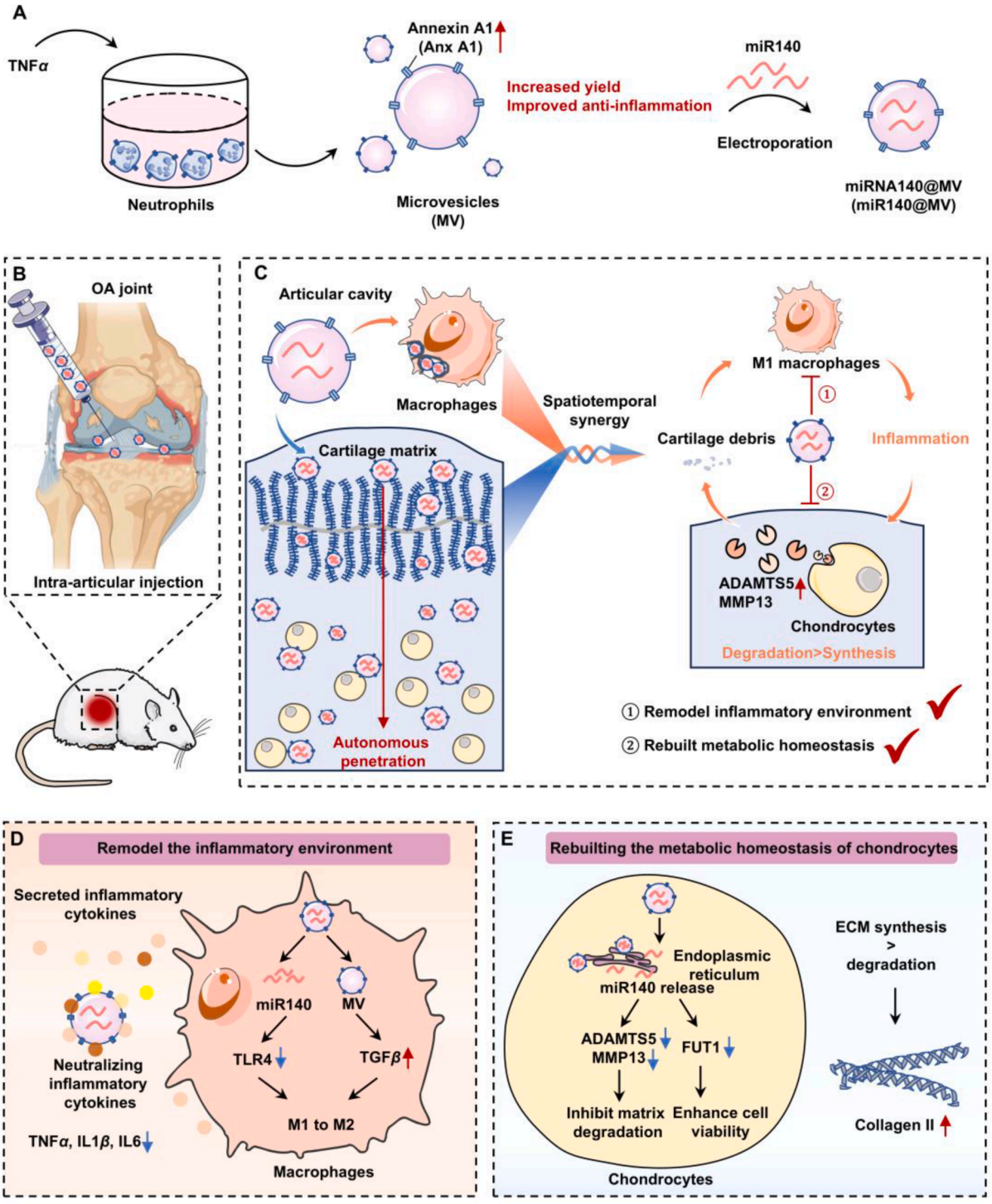

Figure 1 Schematic illustration of the synergized miR140@MVs system for robust OA therapy. (A) Preparation of anti-inflammatory MVs and miR140@MVs. (B) Intra-articular (i.a.) injection of miR140@MVs into DMM mice. (C) miR140@MVs could remodel the inflammatory environment through regulating macrophages in the articular cavity and rebuilding the metabolic of chondrocytes located in the dense cartilage matrix, thus breaking the negative feedback loop mediated by cartilage debris-induced inflammation, finally leading to arresting and even reversing cartilage breakdown. (D) The mechanisms of miR140@MVs on remodeling the inflammatory environment, including adsorbing inflammatory cytokines in the articular cavity and converting macrophages toward anti-inflammatory M2 phenotypes. (E) The mechanisms of miR140@MVs on rebuilding the metabolic homeostasis of chondrocytes through enhanced production and reduced degradation of ECM.

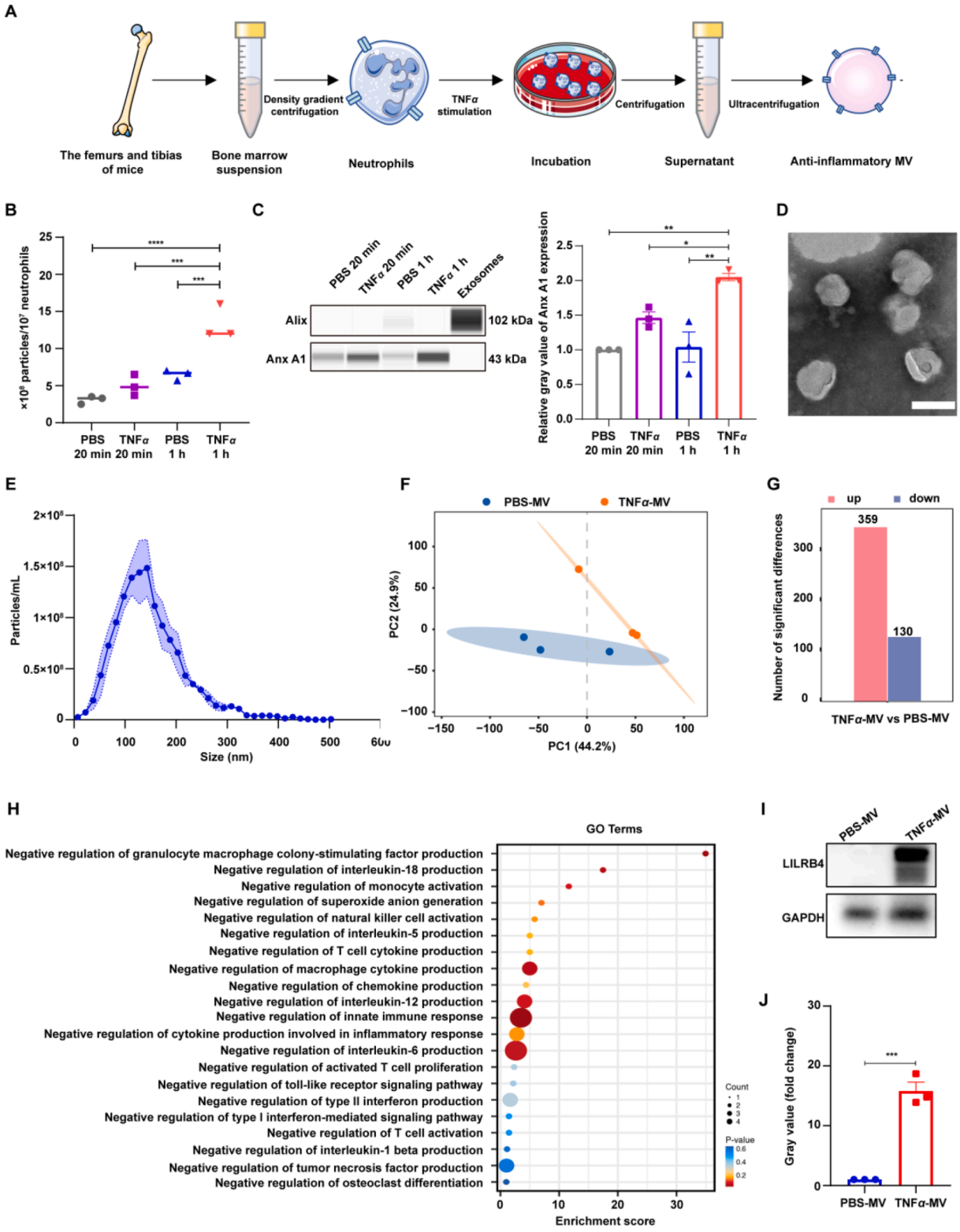

Figure 2 Production of anti-inflammatory MVs. (A) Schematic illustration of the preparation of anti-inflammatory MVs. (B) The yield of MVs from neutrophils that received different treatments. The total amount of protein in each group was 0.8 μg. (C) The expressions of Anx A1 and Alix of MVs were detected by capillary-based protein separation and immunodetection (Simple Western™) and normalization to the PBS controls. Exosomes were used as a control. (D) TEM images of MVs. Scale bars: 100 nm. (E) The size distribution of MVs were analyzed by NTA. The data are shown as mean ± SEM (blue regions), $n = 3$. (F) PCA score plot of proteomics analysis data. (G) Numbers of differentially expressed proteins between TNFα-MVs and PBS-MVs. (H) GO pathway analysis of the differentially expressed genes in the TNFα-MVs *vs.* PBS-MVs. (I) Western blotting analysis of LILRB4 expression in PBS-MVs and TNFα-MVs. GAPDH serves as a loading control. (J) The gray values of LILIRB4 were analyzed by ImageJ. The data are shown as mean ± SEM and analyzed by *t*-test with Tukey's correction, $n = 3$. $^{***}P < 0.001$.

purchased from Absin (Wuhan, China). Anti-MMP13 antibody (ab39012) was bought from Abcam (USA). Anti-FUT1 (A15585) antibody and anti-TLR4 (A11226) antibody were purchased from Abclonal (Wuhan, China). IL1β and TNFα enzyme-linked immunosorbent assay (ELISA) kit was purchased from Elabscience (Houston, TX, USA).

2.3. *Cells*

RAW264.7 cells were purchased from the American Type Culture Collection (ATCC, Manassas, VA, USA). The identities of the cell lines were verified by STR analysis, and the cell lines were confirmed to be mycoplasma-free. The cells were maintained in Dulbecco's Modified Eagle's Medium (DMEM, Hyclone, UT, USA) with 10% fetal bovine serum (FBS, Gibco, CA, USA) and 1% penicillin−streptomycin (Hyclone, UT, USA). To obtain M1 phenotype macrophages, RAW264.7 was treated with LPS (100 ng/mL) (Invitrogen, CA, USA) for 24 h.

L929 mouse fibroblast cells were purchased from the ATCC and grown at 37 °C with 5% CO_2 for 7 days in DMEM supplemented with 10% FBS. Then, the supernatant containing macrophage colony-stimulating factor (M-CSF) was collected and stored at −80 °C for later use. For BMDM culture, tibia and femur bones were harvested bilaterally and bone marrow was flushed out

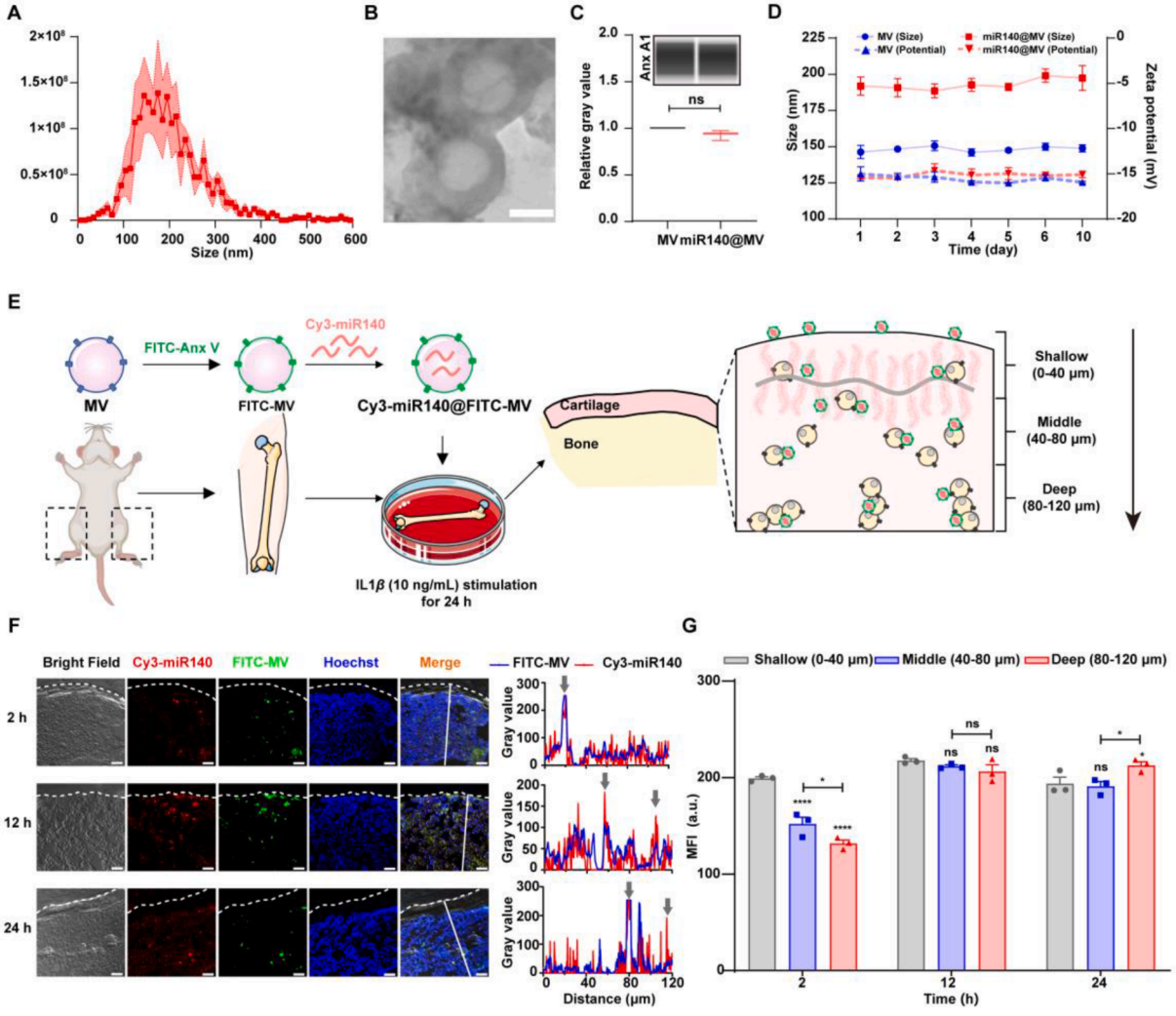

Figure 3 Preparation of miR140@MVs with autonomous cartilage-penetration ability. (A) The size distribution of miR140@MVs was analyzed NTA. The data are shown as mean ± SEM (red regions), $n = 3$. (B) TEM images of miR140@MVs. Scale bars: 100 nm. (C) Capillary electrophoresis immunoassay of Anx A1 expression of MVs and miR140@MVs. The gray value of Anx A1 protein expression normalizes to that of MVs analyzed by Image J. (D) The variations in particle size and zeta potential of MVs and miR140@MVs in PBS at 4 °C for 10 days. (E) Schematic illustration of the preparation and the penetration of miR140@MVs into OA-mimic cartilage. (F) The infiltrability of Cy3-miR140@FITC-MVs in OA-mimic cartilage was observed by confocal laser scanning microscopy (CLSM). miR140 was labeled with Cy3 (Red), while MVs were stained by FITC-Annexin V (Green). The cell nuclei were stained with Hoechst 33342 (Blue). Scale bar: 20 μm. The cartilage edge was indicated by a white dotted line. The gray values of FITC-MVs and Cy3-miR140 were analyzed by Image J in line with the white line. The gray arrow indicated the depth of penetration of Cy3-miR140@FITC-MVs. (G) The mean fluorescence intensity (MFI) of Cy3-miR140 in the different regions of cartilages including the shallow region (0−40 μm), the middle region (40−80 μm), and the deep region (80−120 μm). MFI of the shallow region served as a control. The data are shown as mean ± SEM and analyzed by one-way ANOVA test with Tukey's correction, compared with the Shallow group, $n = 3$. No significance, ns; $^{*}P < 0.05$; $^{***}P < 0.001$; $^{****}P < 0.0001$.

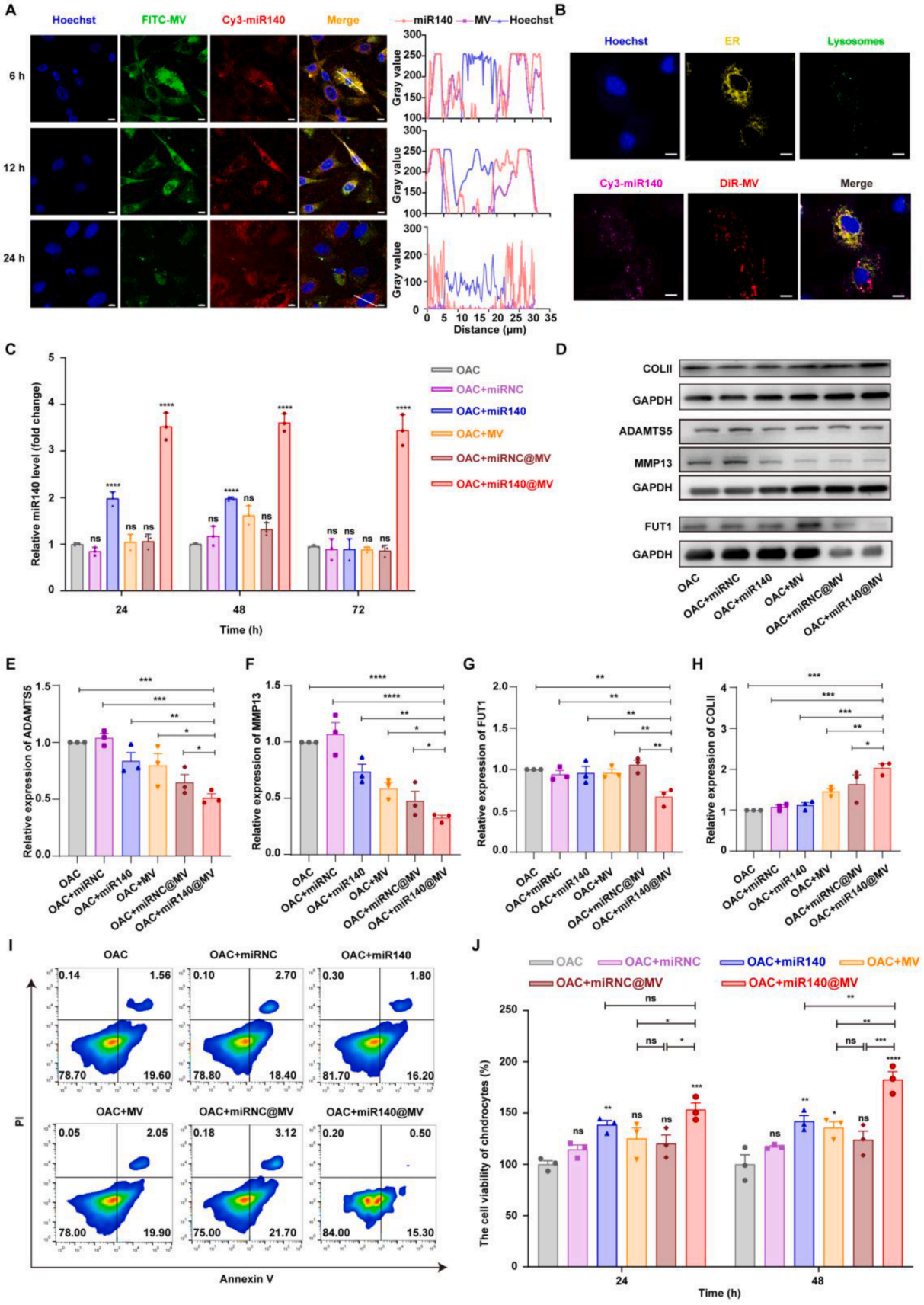

Figure 4 Rebuilding the metabolic homeostasis of OAC by miR140@MVs. (A) The uptake of Cy3-miR140@FITC-MVs by OAC was observed by using CLSM. miR140, MVs and nuclei were separately labeled by Cy3 (Red), FITC-Annexin V (Green) and Hoechst 33342 (Blue).

using a syringe filled with DMEM medium containing 10% FBS. Bone marrow cells were plated in DMEM media with 30% L929 supernatant for 7 days in order to obtain differentiated BMDM. To obtain M1 phenotype macrophages, BMDM obtained at the end of 7 days were treated with LPS (100 ng/mL) for 24 h prior to cell harvesting.

Primary articular chondrocytes were isolated from 5-day-old C57BL/6J mice according to a standard protocol using collagenase II (Yuanye Bio-Technology, Shanghai, China)[36]. Briefly, the proximal end of the femur and the distal end of the tibia were dissected from 5-day-old mice, and ligaments and tendons were excised. Cartilage tissues were incubated with 0.25% trypsin (Thermo Fisher Scientific, Waltham, MA, USA) for 30 min at 37 °C, followed by 12 h digestion with 0.2% type II collagenase. Dissociated cells were seeded on culture dishes. Cells were cultured with DMEM-F12 with 10% FBS. To induce OA chondrocytes (OAC), IL-1β (10 ng/mL) was added for 24 h.

2.4. Isolation and characterization of MVs

Firstly, mature neutrophils were isolated from murine bone marrow using a modified method as reported[37−39]. Briefly, the femurs and tibias of mice were isolated and immersed in RPMI 1640 medium (Hyclone, UT, USA) after removal of the muscle and sinew. Bone marrow was flushed from the bone with phosphate-buffered saline (PBS), followed by centrifugation at 200×g for 3 min (Cence, TG16WS, Hunan, China). The supernatant was removed carefully, and the pellet was re-dispersed into 3 mL of red blood cell lysis buffer. Then the resulting mixture was centrifuged (200×g, 5 min). The obtained cell pellet was re-dispersed into 2 mL of RPMI 1640 medium to obtain the unicellular suspension, which was then added onto a Percoll mixture solution consisting of 55, 65 and 75% (*v/v*) Percoll in PBS, followed by centrifugation at 1000×g for 30 min. The mature neutrophils were recovered at the interface of the 65% and 55% fractions and washed with ice-cold PBS three times. The purity was determined using immunofluorescence double staining with violet 421-conjugated Ly-6G antibody (BioLegend, CA, USA) and phycoerythrin (PE)-conjugated CD11b antibody (BioLegend, CA, USA), and detected by using flow cytometry (Invitrogen, CA, USA). The apoptosis was measured by using immunofluorescence double staining with FITC-conjugated Anx V antibody and PI, and detected by using flow cytometry. The morphology of neutrophils stained with Wright-Giemsa (Jiancheng, Nanjing, China) was observed by an optical microscope (Nikon, Ts2R, Japan).

Next, the isolated neutrophils were resuspended in PBS to a concentration of 1 × 10^7/mL, and TNFα (the final concentration was 50 ng/mL) or the same volume of PBS was added for incubation of 1 h at 37 °C, with 5% CO_2. The cells were centrifuged at 500×g for 3 min at 4 °C, and the supernatant was collected. The supernatant was then centrifuged at 13,000×g for 3 min at 4 °C, and the precipitate was obtained by centrifugation of the supernatant of the previous step at 20,000×g for 1 h at 4 °C (Allegra 64R, Beckman Coulter, CA, USA). Then the MV suspension was obtained by washing three times with PBS and resuspended in PBS. For obtaining exosomes as a control, the supernatant collected after centrifugation at 20,000×g was continually centrifuged at 100,000×g for 3 h to collect and precipitate exosomes[33,35,40,41]. Besides, 2 μL Annexin V-FITC was added to obtain FITC-MVs, while 1 μmol/L DiR was added to obtain DiR-MVs.

For characterization, NTA (Zetaview, Particle Metrix, Germany) was used to detect the size distribution of MVs, and the zeta potential was characterized by a potentiometer (BL-200SM, Brookhaven, USA). Samples were fixed onto copper grids and stained with phosphotungstic acid negative staining for TEM (HT7700, Hitachi, Japan) to analyze the morphology of MVs. 1% (*v/v*) protease inhibitor and RIPA lysate were added to neutrophil MVs or exosomes and lysate on ice for 30 min. After centrifugation at 12,000×g at 4 °C for 15 min, the supernatant was collected. The protein amounts were measured according to the instructions of the BCA protein Quantification Kit (Beyotime Biotechnology, Shanghai, China), and each sample was diluted to the same concentration with a loading buffer. Immunoblotting was performed with Annexin A1 antibody (ab214486, Abcam) and Alix antibody (ab275377, Abcam) on Simple Western™ (USA) using buffer kits with protein separation range from 12 to 230 kDa according to the instructions. Compass software (ProteinSimple, CA, USA) was used for analysis.

For Proteomics analysis, the PBS-MVs and TNFα-MVs were lysed by RIPA lysis buffer supplemented with 1 mmol/L PMSF. Then samples were further lysed with sonication. The parameters were set as 1s/1s intervals and 80 W for 2 min. After sonication, the samples were centrifuged at 12,000×g for 10 min at 4 °C to remove insoluble particles, and repeated once to further exclude precipitation. Protein concentration was determined by BCA assay to satisfy the requirements of proteomics. Each component underwent separation using the nanoElute liquid chromatography system by Oebiotech (Shanghai, China). Mobile phase A consisted of a 0.1% formic acid solution in water, while mobile phase B contained 0.1% formic acid in acetonitrile. The gradient elution conditions were as follows: 0−45 min, 2%−22% B; 45−50 min, 22%−37% B; 50−55 min, 37%−80% B; 55−60 min, 80%. Subsequent to chromatographic separation by the ultra-high-performance liquid chromatography system, the peptides were injected into the timsTOF Pro mass spectrometer manufactured by Bruker for analysis. The mass spectrometry parameters were set as follows: the capillary voltage was maintained at 1500 V, with primary and secondary scan ranges spanning from 100 to 1700 m/z, and ion mobility windows ($1/K_0$) ranging from 0.7 to 1.3 Vs/cm^2.

Scale bar: 5 μm. The gray values were analyzed by Image J followed by the white lines. (B) The distribution of Cy3-miR140@FITC-MVs within OAC was observed by ultra-high resolution confocal microscope (Leica, Stellaris 5) at 6 h co-incubation. ER and lysosomes were labeled by ER-Tracker (Yellow) and Lyso-Tracker (Green). Scale bar: 5 μm. (C) The relative level of miR140 in OAC after incubation with different formulations. The data are shown as mean ± SEM and analyzed by one-way ANOVA test with Tukey's correction, $n = 3$. OAC without treatment served as a control. No significance, ns; ****$P < 0.0001$. (D) Western blotting of COLII, ADAMTS5, MMP13 and FUT1 in OAC treated with miR140@MVs. The gray values of (E) ADAMTS5, (F) MMP13, (G) FUT1 and (H) COLII in (D) were analyzed by Image J and normalized to their respective baseline controls. The data are shown as mean ± SEM and analyzed by one-way ANOVA test with Sidak's correction, $n = 3$. No significance, ns; *$P < 0.05$; **$P < 0.01$; ***$P < 0.001$; ****$P < 0.0001$. (I) The representative flow cytometry diagram of apoptosis ratios of OAC treated with different formulations. (J) The viability of OAC after different treatments was detected by cell counting kit (CCK)-8. The data are shown as mean ± SEM and analyzed by one-way ANOVA test with Tukey's correction, $n = 3$. OAC served as a control. No significance, ns; *$P < 0.05$; **$P < 0.01$; ***$P < 0.001$; ****$P < 0.0001$.

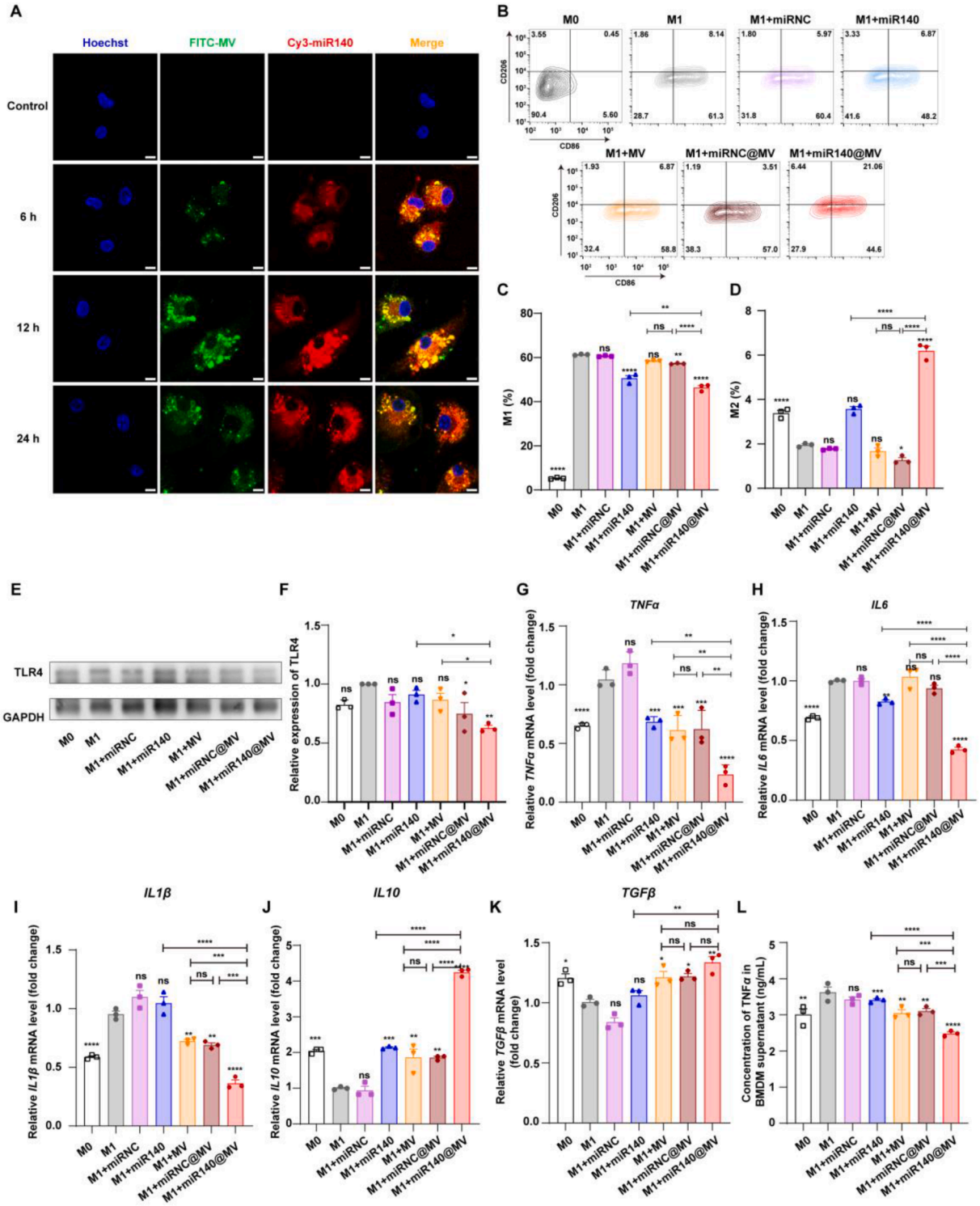

Figure 5 miR140@MVs inhibit the pro-inflammatory effect of LPS-induced BMDM *in vitro*. (A) The intracellular location of Cy3-miR140@FITC-MVs in BMDM cells stimulated with LPS (100 ng/mL) for 24 h (M1 macrophages). miR140 is labeled with Cy3 (Red) and MVs are stained by FITC-Annexin V (Green). The nuclei were stained by Hoechst 33342 (Blue). Scale bar: 5 μm. (B) Representative flow cytometric analysis of BMDM treated with different formulations. The (C) M1 ($CD86^+CD206^-$) and (D) M2 ($CD86^-CD206^+$) phenotypes were analyzed by Flowjo. The data are shown as mean ± SEM and analyzed by one-way ANOVA test with Tukey's correction, compared with M1 group. $n = 3$. No significance, ns; $^*P < 0.05$; $^{**}P < 0.01$; $^{****}P < 0.0001$. (E) Western blotting of TLR4 in LPS-induced BMDM treated with different formulations. (F) The relative expression of the protein band was analyzed by Image J and normalized to its respective baseline controls. The data are shown as mean ± SEM and analyzed by one-way ANOVA test with Tukey's correction, $n = 3$. $^*P < 0.05$. The relative mRNA levels of (G) *TNFα*, (H) *IL6*, (I) *IL1β*, (J) *IL10*, (K) *TGFβ* in LPS-induced BMDM receiving different formulations. The data are shown as mean ± SEM and analyzed by one-way ANOVA test with Tukey's correction, compared with the M1 group, $n = 3$. No significance, ns; $^*P < 0.05$; $^{**}P < 0.01$;

2.5. Preparation of miR140@MVs

Freshly isolated MVs (2 μg) were resuspended in PBS and added into the well of electroporation plates, followed by the addition of 5 pmol of Cy3-miR140. After electroporation, the samples were collected from each well, centrifuged at 20,000×*g* at 4 °C for 1 h, and the supernatant was collected. The fluorescence of the supernatant was detected by a microplate reader (Cytation, Biotek, USA) with an excitation wavelength of 532 nm and an emission wavelength of 580 nm. The fluorescence standard curve of Cy3-miR140 was drawn. The content of Cy3-miR140 in the supernatant can be calculated according to the fitting formula. The electroporation efficiency was calculated according to Eq. (1):

$$\text{Electroporation efficiency}\ (\%) = (\text{Total molar of Cy3}-\text{miR140} - \text{Supernatant molar of Cy3}-\text{miR140})/\ \text{Total molar of Cy3}-\text{miR140} \times 100 \quad (1)$$

For drug loading efficiency, Cy3-miR140@MVs was lyophilized at first. Then, 100 μL of PBS containing 1% Triton X-100 was added, followed by transferring to a 96-well plate for detection of the fluorescence intensity of Cy3-miR140 by microplate analyzer. The drug loading of Cy3-miR140 in MVs was calculated according to Eq.(2):

$$\text{Drug loading}\ (\%) = \text{Weight of Cy3}-\text{miR140 in Cy3}-\text{miR140@MVs after lyophilization}/\ \text{Weight of Cy3}-\text{miR140@MVs after lyophilization} \times 100. \quad (2)$$

The chondrocytes were placed into six-well plates at a density of 1×10^6 cells/well, and cultured for 24 h in DMEM high glucose medium containing IL1β (10 ng/mL). After incubation with Cy3-miR140@MVs for 24 h, the uptake of chondrocytes was detected by flow cytometry (Invitrogen, CA, USA).

2.6. Penetration of miR140@MVs in cartilage explant

Cartilage explants were isolated from C57BL/6J male mice. After treatment with IL1β for 24 h, a total of 5 nmol/L Cy3-miR140, Cy3-miR140@FITC-MVs and DiO-MC3-LNP was added to the culture medium of cartilage explants for another incubation of 24 h at 37 °C and 5% CO_2. Then, cartilage explants were washed with PBS and sectioned to 8 μm thickness by using a freezing microtome (Leica Biosystems). Sections were placed on glass slides and immediately observed under a CLSM (LSM 880, ZEISS). Quantitative analysis was performed on ImageJ.

2.7. Intracellular transport of miR140@MVs

For intracellular transport observation, LPS-induced RAW264.7, BMDM or IL1β-induced chondrocytes were placed onto cell culture imaging dishes (Thermo Fisher Scientific, Waltham, MA, USA). Then, Cy3-miR140@FITC-MVs were added at a concentration of miR140 of 50 nmol/L. After incubation for 24 h at 37 °C in 5% CO_2 incubator, the cells were observed by CLSM or 3D cell explorer (Nanolive, Switzerland).

As for subcellular localization analysis, chondrocytes were incubated with Cy3-miR140@DiR-MVs for 6 h, washed with PBS, and sequentially stained with ER-Tracker (1:1000, Beyotime) and LysoTracker (1:2000, Yeasen) for 30 min at 37 °C, followed by Hoechst 33342 (1:2000, Beyotime) nuclear staining for 5 min. Next, cells were washed with PBS for three times. High-resolution imaging was performed on Leica STELLARIS 5 confocal microscope.

2.8. Regulation of OAC via miR140@MVs

OAC were seeded into 96-well or 6-well plates at a density of 2000 cells/well or 1×10^6 cells/well with the addition of PBS, miRNC, miR140, MVs, miRNC@MVs or miR140@MVs (miR140 concentration, 50 nmol/L) for incubation for different times at 37 °C in 5% CO_2 incubator. Then, the supernatant was discarded and the cells were washed with PBS three times for further detection.

The proliferation and apoptosis of OAC were evaluated by CCK-8 assay (Beyotime Biotechnology, China) and apoptosis kit (Vazyme, China) according to the manufacturer's instructions.

For the qPCR assay, the cells were collected after 24 h treatment. Briefly, RNA was isolated using RNA isolater Total RNA Extraction Reagent (Vazyme, Nanjing, China) according to the vendor's protocol. The RNA was transformed to cDNA using a HiScript III 1st Strand cDNA Synthesis Kit (Vazyme, Nanjing, China). After that, real-time qPCR was performed with different genes of interest. All the primers are shown in Supporting Information Table S1.

For Western blotting, the cells were collected after 24 h treatment. The total protein was harvested in radioimmunoprecipitation assay (RIPA) buffer (Cat#P0013B, Beyotime Biotechnology, Shanghai, China), supplemented with the protease inhibitor phenylmethanesulfonyl fluoride (PMSF) (Cat#P1005-1, Beyotime Biotechnology, China). The protein concentration was detected using the BCA Protein Assay Kit (Beyotime Biotechnology, China). The obtained proteins were separated by means of sodium dodecyl sulfate-polyacrylamide gel electrophoresis (SDS-PAGE) and then transferred onto polyvinylidene fluoride (PVDF) membranes using a *trans*-buffer at 100 V for 90 min. The

$^{***}P < 0.001$; $^{****}P < 0.0001$. (L) The TNFα level in LPS-induced BMDM supernatant was detected by ELISA assay. The data are shown as mean ± SEM and analyzed by one-way ANOVA test with Tukey's correction, $n = 3$. No significance, ns; $^{**}P < 0.01$; $^{***}P < 0.001$; $^{****}P < 0.0001$. (F–I) Values are normalized to the M1 (baseline control) group.

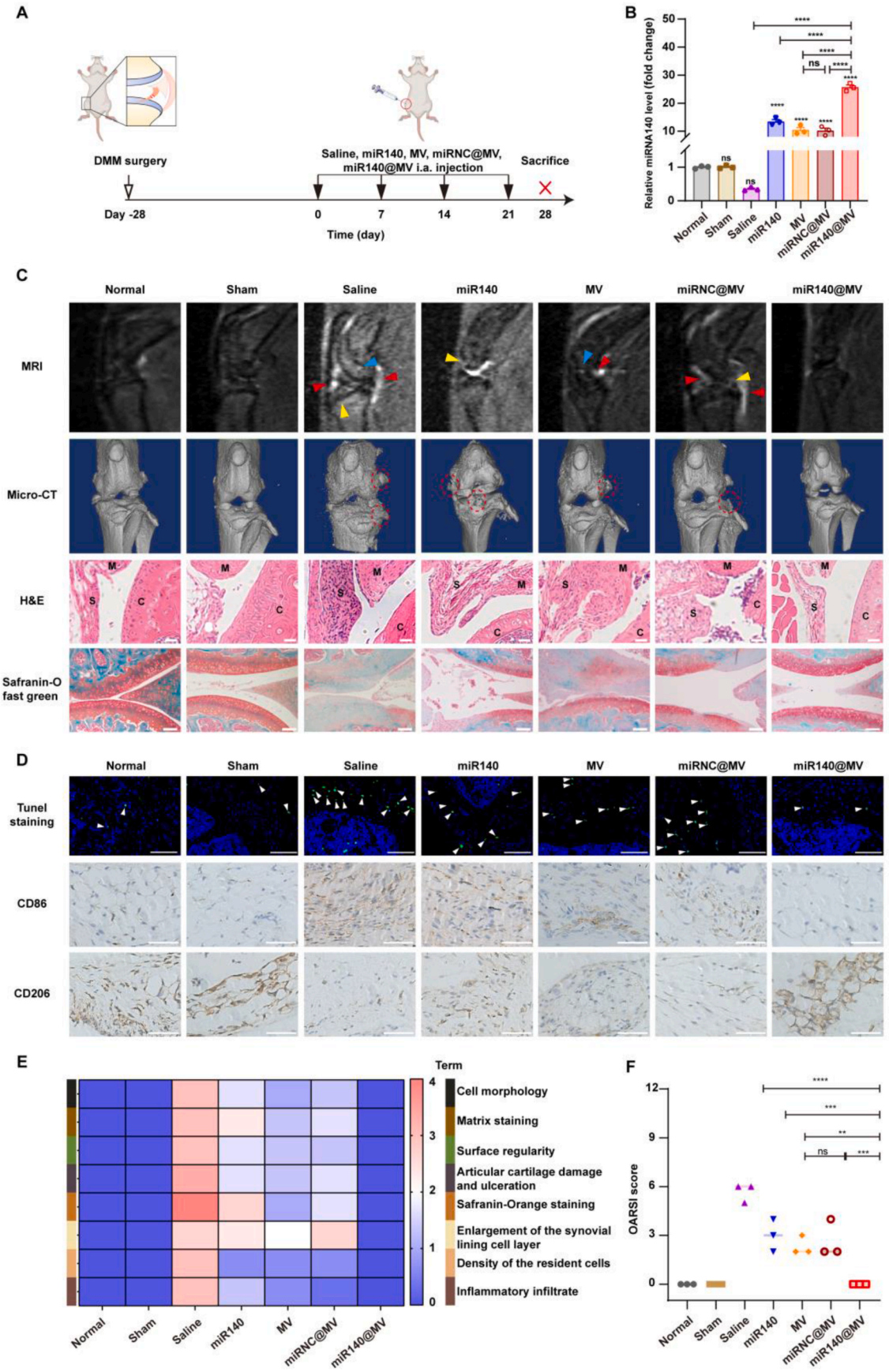
A
DMM surgery
Saline, miR140, MV, miRNC@MV, miR140@MV i.a. injection
Sacrifice
Day -28
0
7
14
21
28
Time (day)
B
Relative miRNA140 level (fold change)
Normal
Sham
Saline
miR140
MV
miRNC@MV
miR140@MV
C
Normal
Sham
Saline
miR140
MV
miRNC@MV
miR140@MV
MRI
Micro-CT
H&E
Safranin-O fast green
D
Tunel staining
CD86
CD206
E
Term
Cell morphology
Matrix staining
Surface regularity
Articular cartilage damage and ulceration
Safranin-Orange staining
Enlargement of the synovial lining cell layer
Density of the resident cells
Inflammatory infiltrate
F
OARSI score

membranes were incubated overnight at 4 °C with the primary antibodies including ADAMTS5 (abs116232, Absin, China), MMP13 (ab39012, Abcam, USA), FUT1 (A15585, Abclonal, China), Collagen II (abs131559, Absin, China) and Glyceraldehyde-3-phosphate dehydrogenase (GAPDH) (abs132004, Absin, China). Of which, GAPDH was used to normalize the relative protein expression. Then, the membranes were washed with Tris Buffered Saline with Tween-20 (TBST) three times, followed by incubation with HRP Goat Anti-rabbit IgG (H + L) antibody (Cat#abs20147, absin, China) for 1 h at RT. After washing with TBST for 30 min, the membranes with the proteins were visualized by means of the Super ECL kit (Cat#36208ES76, Yeasen, Shanghai, China).

2.9. Regulation of macrophages via miR140@MVs

Macrophages were stained with APC-Anti CD86 (105011, Biolegend, USA) and Alexa Fluor®488-Anti CD206 (C068C2, Biolegend, USA) for 20 min at room temperature. Isotype controls were performed using APC-conjugated rabbit IgG (Abclonal, A24173). The expression of CD86 and CD206 on the surface of macrophages was detected by flow cytometry. The qPCR and Western blotting assay used the same method as above. The prime sequences are shown in Table S1.

2.10. Adsorption of inflammatory factors

The adsorption of inflammatory factors by MVs was detected by ELISA assay. MVs and miR140@MVs (the final concentration of miR140 was 50 nmol/L) were mixed with recombinant mouse TNFα or mouse IL1β at final concentrations ranging from 0 to 20 ng/mL. The mixtures were incubated for 4 h at 37 °C and then centrifuged at 20,000×g for 1 h to remove the MVs and miR140@MVs. Cytokine concentration in the supernatant was quantified by mouse TNFα or mouse IL1β enzyme-linked immunosorbent assay (ELISA) kits (Elabscience, USA).

2.11. Construction of DMM mice model

The mice were anesthetized with isoflurane and fixed. The incision was made in the medial patellar ligament of the right knee of the mice under the asana microscope. The joint capsule was opened and the medial meniscus was found between the femur and tibia. After 28 days, the destabilization of the medial meniscus mice model was completed[42].

2.12. OA therapy efficacy via miR140@MVs on DMM mice

For multiple intra-articular injections, DMM mice were randomly divided into 5 groups (5 mice in each group), which received different formulations including: (1) saline (20 μL/mouse); (2) miR140 (700 pmol/mouse, 20 μL/mouse); (3) MVs (1.5 μg/mouse, 20 μL/mouse); (4) miRNC@MVs (1.5 μg MV/mouse, 20 μL/mouse); (5) miR140@MVs (1.5 μg MV/mouse, 20 μL/mouse), once a week for a total of four times.

For one-month efficacy evaluation, DMM mice were randomly divided into 3 groups (5 mice in each group), which received different formulations including: (1) single saline injection (20 μL/mouse); (2) multiple miR140@MVs injections (1.5 μg MV/mouse, once a week for a total of four times); (3) single miR140@MVs injection (1.5 μg MV/mouse).

All endpoint was set at the 28th day after the first administration. Meanwhile, healthy mice (Normal) purchased together with the above DMM mice were used as a normal control. The sham operation mice (Sham) with only the joint capsule incision were constructed for comparison.

For MRI and micro-CT imaging, the parameters of MRI were set as follows: Echo time = 33 ms,repeat time = 2500 ms, flip angle = 180°; while that of the micro-CT were: scanning resolution = 18 μm, voltage = 70 kV, electric current = 114 μA. 3D knee reconstruction was performed using Mimics 17.0 software (Materialise).

For histopathology, the anterior and posterior tissues were embedded in the same cassette in paraffin and sectioned into a number of 5 μm frontal sections within the joint. Sections were stained with H&E or safranine O/fast green, and the section containing the most severe medial tibial lesion was identified by a blinded investigator for scoring. Gross pathological scoring followed the published guidelines of the OARSI Histopathology. Semiquantitative synovial inflammation grading also followed OARSI guidelines.

2.13. In vivo imaging

DMM mice were randomly divided into 3 groups (with 5 mice in each group), which received different formulations including: (1) Cy5-miR140 (700 pmol/mouse), (2) DiR-MVs (1.5 μg/mouse), (3) Cy5-miR140@DiR-MVs (1.5 μg/mouse, equivalent to 700 pmol/mouse of miR140). The formulations were injected into the right knee cavity and photographed under the *in vivo* imaging system for 28 days.

Cryosection of cartilage tissues was done by following a standard procedure. Briefly, the tissue samples were thawed, mounted, and refrozen in OCT (optimum cutting temperature compound) embedding media, followed by cryosection into 6 μm-thick sections using a freezing microtome (Leica). Sections were either refrozen and stored at low temperatures (−25 °C) or detected immediately. The nuclei were stained with Hoechst 33342. The chondrocytes were stained with ColII antibody and the second antibody

Figure 6 *In vivo* therapeutic efficacy of miR140@MVs after repeated i.a. injections. (A) Schematic illustration of the administration regimen. (B) The relative miR140 level in the whole-knee joint of DMM mice treated with different formulations. The data are shown as mean ± SEM and analyzed by one-way ANOVA test with Tukey's correction, $n = 3$. The normal group served as the control. No significance, ns; ****$P < 0.0001$. (C) Typical images of imageological examinations and histological analysis. Red arrows: synovial inflammation; Yellow arrows: cartilage defect; Blue arrows: bone marrow edema; Red circles: periarticular osteophytes; M: meniscus; S: synovial; C: cartilage. Scale bar: 100 μm. (D) TUNEL staining and immunohistochemical analysis of CD86 and CD206 in the sections of cartilage from the knees of DMM mice receiving various treatments. White arrows: apoptotic chondrocytes. Scale bar: 50 μm. (E) Heatmap of variables of histological scoring in each group. (F) OARSI grades of the mice joints in each group. The data are shown as mean ± SEM and analyzed by one-way ANOVA test with Tukey's correction, $n = 3$. The normal group served as the control. No significance, ns; **$P < 0.01$; ***$P < 0.001$; ****$P < 0.0001$.

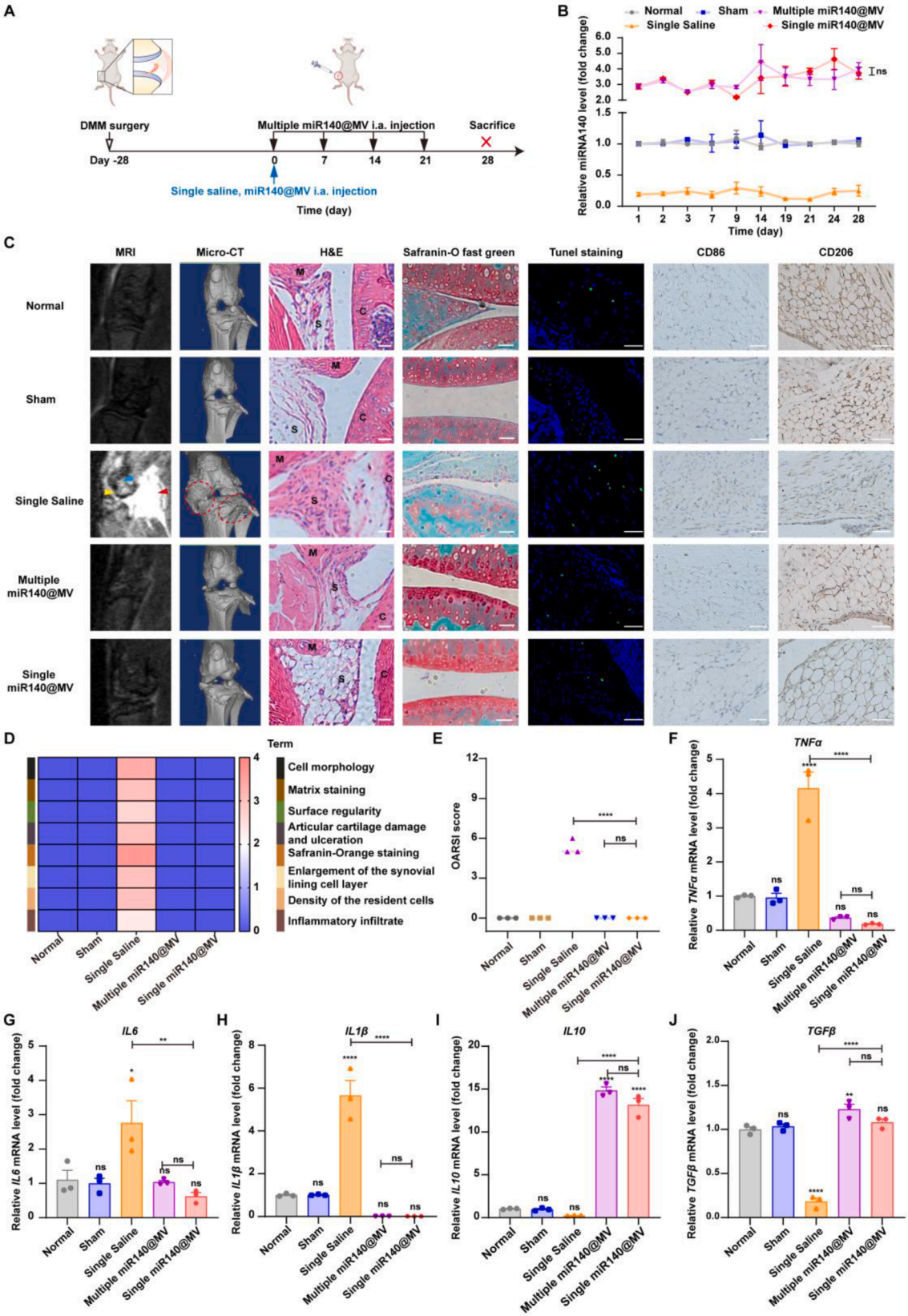

Figure 7 Single miR140@MVs for prolonged OA treatment. (A) Schematic illustration of the administration regimen. (B) The relative miR140 level in the whole-knee joint of DMM mice treated with different formulations for 28 days. The data are shown as mean ± SEM and analyzed by one-way ANOVA test with Tukey's correction, $n = 3$. The normal group served as the control. No significance, ns. (C) Typical images of imageological examinations, histological analysis, TUNEL staining and immunohistochemical analysis. Red arrows: synovial inflammation;

(ab150113, Abcam). As for synovium tissues, the macrophages were stained with F4/80 antibody (123119, Biolegend, USA).

2.14. Statistical analysis

The results are presented as mean ± standard error of the mean (SEM) as indicated. These data were compared by Student's *t* test between two groups and ordinary one-way analysis of variance (ANOVA) for three or more groups. All statistical analyses were conducted by the GraphPad Prism software. The threshold of a statistically significant difference was defined as $^{*}P < 0.05$, $^{**}P < 0.01$, $^{***}P < 0.001$, $^{****}P < 0.0001$, and ns as no significance.

3. Results

3.1. Production of anti-inflammatory MVs via an immune-stimulation method

To prove the idea, we firstly upgraded the production approach of MVs as schemed in Fig. 2A. Neutrophils were isolated from mice bone marrow by density gradient centrifugation according to our previous studies[37−39,43], which showed a purity of 91.6% and a viability higher than 90%, along with the typical lobular-shaped nuclei stained by Giemsa-Wright (Supporting Information Fig. S1). As reported, Anx A1, the membrane protein of neutrophils, acts as the major anti-inflammatory effect through regulating the macrophages, which is also a well-established MV-specific marker[44]. Thus, improving the Anx A1 level of neutrophils would favor the anti-inflammatory effect of MVs which bud from the neutrophils. Herein, TNFα with optimal concentration and incubation time was applied to stimulate neutrophils to produce MVs with high yield and improved Anx A1 level. We demonstrated that the yield of MVs was about 1.3×10^9 particles per 10^7 neutrophils *via* nanoparticle tracking analysis (NTA) and a total of 33.4 μg *via* bicinchoninic acid assay (BCA), about 1.6-fold and 1.9-fold higher than that by the common production method (PBS treatment), respectively (Fig. 2B and Supporting Information Table S2). Notably, the obtained MVs exhibited an extremely high level of Anx A1 protein but no Alix protein (the typical exosome marker)[45] by using Simple Western™, further confirming the effectiveness of TNFα stimulation for MVs production with improved purity (Fig. 2C and Supporting Information Fig. S2). Meanwhile, these MVs displayed a cup-shaped morphology observed by transmission electron microscopy (TEM; Fig. 2D), with an average diameter of 142.0 ± 4.5 nm (Fig. 2E) and zeta potential of −15.0 ± 1.4 mV (Table S2) by NTA. Different from MVs, exosomes appeared as homogeneous 20−30 nm spheres by TEM (Supporting Information Fig. S3A and S3B), and a peak size of 103 nm by NTA (Fig. S3C). Notably, the amount of MVs exceeded exosomes by 10-fold, suggesting the effectiveness of the production approach of MVs with high purity and yield.

Moreover, we conducted a comprehensive proteomic analysis of MVs derived from neutrophils stimulated by TNFα (TNFα-MVs) to understand the effect of TNFα stimulation on MVs, in comparison to those without stimulation (PBS-MVs). Principal component analysis (PCA) showed that there were two distinguishable patterns of proteins (Fig. 2F), indicating the significant difference in protein levels between TNFα-MVs and PBS-MVs. To be specific, a total of 489 proteins was differentially expressed using the cutoff value of a two-fold change and a *P*-value<0.05, of which 359 proteins were upregulated and 130 proteins were downregulated (Fig. 2G). On the basis of gene ontology (GO) enrichment analysis (Fig. 2H), the TNFα-MVs displayed functional enrichment in biological processes related to negative regulation of innate immune response and inflammatory factor production, such as IL1β, IL6, IL12, IL5, interferons and TNFα. From the proteomic profile, we found that leukocyte immunoglobulin-like receptor subfamily B member 4 (LILRB4) was significantly upregulated, confirmed by Western blotting with a 15-fold increase in TNFα-MVs than that in MVs (Fig. 2I and J, Supporting Information Fig. S4). LILRB4—a receptor known to significantly suppress the production of inflammatory cytokines like TNFα in macrophages[46]—strongly supports the inherent anti-inflammatory properties of TNFα-MVs. It can be speculated that LILRB4 serves as a potential mechanism contributing to the immunomodulatory function of MVs, which we would further investigate in the future.

Taken together, we have established the production approach of anti-inflammatory MVs *via* an immune-stimulation method, holding the potential as promising vectors for miR-140 delivery in OA treatment.

3.2. Preparation and characterization of miR140@MVs with autonomous cartilage-penetration ability

Based on the anti-inflammatory MVs, miR140@MVs were prepared by encapsulating miR140 into MVs *via* electroporation. We firstly optimized the feeding ratio of miR140 and MVs. When the ratio of Cy3-miR140 and MVs was 800 pmol/μg, miR140@MVs achieved a relatively high encapsulation efficiency of 56.39% (Supporting Information Fig. S5). The obtained miR140@MVs revealed a median diameter of about 191.9 ± 10.8 nm (Fig. 3A), with a zeta potential of −15.4 ± 0.3 mV (Supporting Information Table S3). Compared with MVs, miR140@MVs showed a larger particle size and similar zeta potential by NTA, and a plump spherical structure by TEM (Fig. 3B), suggesting the encapsulation of miR140. Notably, the electroporation process used had no influence on the Anx A1 expression and population of MVs (Fig. 3C and Table S3). In addition, both MVs and miR140@MVs in PBS at 4 °C maintained stable particle size and zeta potential for at least 10 days (Fig. 3D), which was beneficial for future applications.

The autonomous penetration ability of MVs in the dense, avascular, and cell-impenetrable cartilage matrix acts as the precondition for effective miRNA delivery. To assess this, mouse

Yellow arrows: cartilage defect; Blue arrows: bone marrow edema; Red circles: periarticular osteophytes. M: meniscus; S: synovial; C: cartilage. Scale bars in H&E and safranine O-fast green staining: 100 μm; in TUNEL staining and immunohistochemical analysis: 50 μm. (D) Heatmap of variables of histological scoring in each group. (E) OARSI grades of the mice joints in each group. The data are shown as mean ± SEM and analyzed by one-way ANOVA test with Tukey's correction, $n = 3$. The normal group served as the control. No significance, ns; $^{****}P < 0.0001$. (F−J) The relative mRNA levels of inflammatory factors in OA joints from mice after different treatments, including (F) *TNFα*, (G) *IL6*, (H) *IL1β*, (I) *IL10* and (J) *TGFβ*. The data are shown as mean ± SEM and analyzed by one-way ANOVA test with Tukey's correction, $n = 3$. The normal group served as control. No significance, ns; $^{**}P < 0.01$; $^{****}P < 0.0001$.

cartilage explants were treated with IL1β to mimic the OA-affected cartilage, which was then incubated with Cy3-miR140@FITC-MVs to trace the migration in the OA-affected cartilage (Fig. 3E). We observed that the overlapped yellow fluorescence of Cy3-miR140@FITC-MVs migrated to the deep region (80−120 μm) of cartilage for 24 h (Fig. 3F and G). While the control groups of free miR140 and MC3-LNP (the typical formulation of LNP) at 24 h co-incubation exhibited limited cartilage penetration (Supporting Information Fig. S6), significantly less than miR-140@MVs. The comparative data further demonstrated the superior autonomous penetration capacity of MVs.

In short, these data suggest that miR140@MVs can effectively penetrate into the cartilage in a miR140-encapsulated manner over time, which favors the following cellular uptake by chondrocytes discretely distributed in cartilage.

3.3. *miR140@MVs rebuild the metabolic homeostasis of osteoarthritis chondrocytes*

Before exploring the effect of miR140@MVs on osteoarthritis chondrocytes (OAC), we performed to examine whether miR140@MVs could enter OAC and the biodistribution within OAC *in vitro*. As shown in Fig. 4A, Cy3-miR140@FITC-MVs displayed an overlapped yellow fluorescence within OAC, indicating the valid entrapment of miR140@MVs by OAC. After incubation for 24 h, most of the red fluorescence of Cy3-miR140 was distributed in the cytoplasm of OAC in separation from the green fluorescence of MVs, suggesting the successful release of miR140 from MVs to the chondrocyte cytoplasm, which was essential for gene silencing. The successful release of miR140 from MVs was further confirmed by the 3D live cell imaging systems. Notably, we found that Cy3-miR140@FITC-MVs and diffused Cy3-miR140 localized near ER (Supporting Information Fig. S7). For clarity, an ultra-high resolution confocal microscope (Leica, Stellaris 5) was applied to observe the location of Cy3-miR140@FITC-MVs within OAC (Fig. 4B). We found that about 45% of Cy3-miR140 fluorescence was colocalized with ER-Tracker, confirming the efficient delivery of miR140 *via* MVs to the ER vicinity. While minimal overlap (∼7% colocalization) was observed between Cy3-miR140@FITC-MVs and LysoTracker, indicating negligible lysosomal entrapment. The successful delivery of miR140 *via* MVs to ER as the RNAi translation machinery[47,48] showed the potential for effective regulation of target genes.

Furthermore, miR140@MVs upregulated nearly 1.7-fold level of miR140 in OAC compared with free miR140 measured by quantitative reverse transcription-polymerase chain reaction (qPCR) (Fig. 4C). The high level of miR140 *via* MVs delivery in OAC was maintained at least 72 h, while free miR140 decreased gradually. These data suggested the effective and prolonged complement of miR140 into OAC *via* the delivery of miR140@MVs.

Subsequently, we sought to determine whether the supplementary miR140 took effect in OAC. As reported, miR140 holds the capability of inhibiting multiple genes to intervene in the metabolic imbalance of OAC, including *ADAMTS-5* and *MMP-13*[49], two critical catabolic enzymes responsible for the degradation of type II collagen (COL II) and aggrecan, as well as fucosyltransferase 1 (FUT1) associated with the apoptosis of chondrocytes[23]. We demonstrated that miR140@MVs significantly decreased 64%, 59%, and 89% of the levels of *ADAMTS5*, *MMP13* and *FUT1* mRNA, respectively (Supporting Information Fig. S8). A similar tendency could be found in the Western blotting of about 49%, 68% and 33% inhibition on the respective protein expressions of ADAMTS5, MMP13 and FUT1 (Fig. 4D−G, Supporting Information Figs. S9 and S10). Moreover, the expression of COL II was potentiated in OAC treated with miR140@MVs (Fig. 4D and H, Supporting Information Fig. S11), reflecting that miR140@MVs enhanced the synthesis of COL II. Of which, MVs themselves held the capability of promoting COL II synthesis (Fig. 4D and H), which lent a hand to relieve the cartilage damage. We further explored the regulation of miR140@MVs on apoptosis and proliferation of OAC, and demonstrated that miR140@MVs significantly inhibited the apoptosis (Fig. 4I and Supporting Information Fig. S12) and upregulated approximately 1.5-fold of the cell viability at 48 h (Fig. 4J). These results suggested that miR140@MVs effectively downregulated multiple targeted genes related to miR140, thus enhancing the viability of OAC and therefore increasing the synthesis of COL II, but decreasing the release of degradation enzymes.

Taken together, miR140@MVs successfully deliver miR140 to the ER of OAC, followed by effective multiple gene regulation, leading to the redressed metabolic homeostasis of OAC, which potentially makes for arresting and reversing the cartilage breakdown.

3.4. *miR140@MVs present effective anti-inflammation effects through regulating macrophage phenotype and adsorbing inflammatory factors*

Synovium inflammation serves as a typical symptom of OA, which induces the aggravation of cartilage damage owing to the inflamed environment that further disorders the physiological function of OAC[50]. The massively infiltrated macrophages primarily present as the pro-inflammatory M1 phenotype that would exacerbate OA progression by secreting various inflammatory factors[51,52]. Here, we validated that miR140@MVs held the anti-inflammatory ability on both lipopolysaccharide (LPS) treated bone marrow derived macrophages (BMDM) and RAW264.7 cells as M1 macrophages. After endocytosis by M1 macrophages, Cy3-miR140 gradually diffused in macrophage cytoplasm as the incubation time prolonged (Fig. 5A and Supporting Information Fig. S13A), indicating the successful delivery of miR140 to M1 macrophages *via* MVs. Subsequently, miR140@MVs reduced M1 proportion ($CD86^+CD206^-$) by 25% and increased M2 ($CD86^-CD206^+$) ratio by 3-fold in BMDM, compared with M1 group (Fig. 5B−D). A similar tendency could be found in RAW264.7 cells (Fig. S13B−S13D and Supporting Information Fig. S14), further confirming the phenotype conversion of macrophages from M1 towards M2. This conversion of macrophage phenotype can be ascribed to the downregulation of TLR4 on M1 macrophages silenced by miR140 (Fig. 5E and F, Fig. S13E and S13F, Supporting Information Fig. S15−S18). For further confirmation, we detected the levels of inflammatory factors within macrophages and in the supernatant, respectively. The qPCR results showed that the pro-inflammatory factors including *TNF*α, *IL-6* and *IL1*β exhibited respective 77%, 57% and 64% decreases in LPS-induced BMDM treated by miR140@MVs, while the anti-inflammatory factors of *IL10* and transforming growth factor (TGF)-β showed a 4.25-fold and 1.34-fold increase, respectively, compared to that of control (Fig. 5G−K). Additionally, the TNFα production from LPS-induced BMDM was obviously reduced after the miR140@MVs treatment (Fig. 5L). Similar results in LPS-induced RAW264.7 cells further confirmed the polarization effect on macrophages of miR140@MVs (Fig. S13G−S13L).

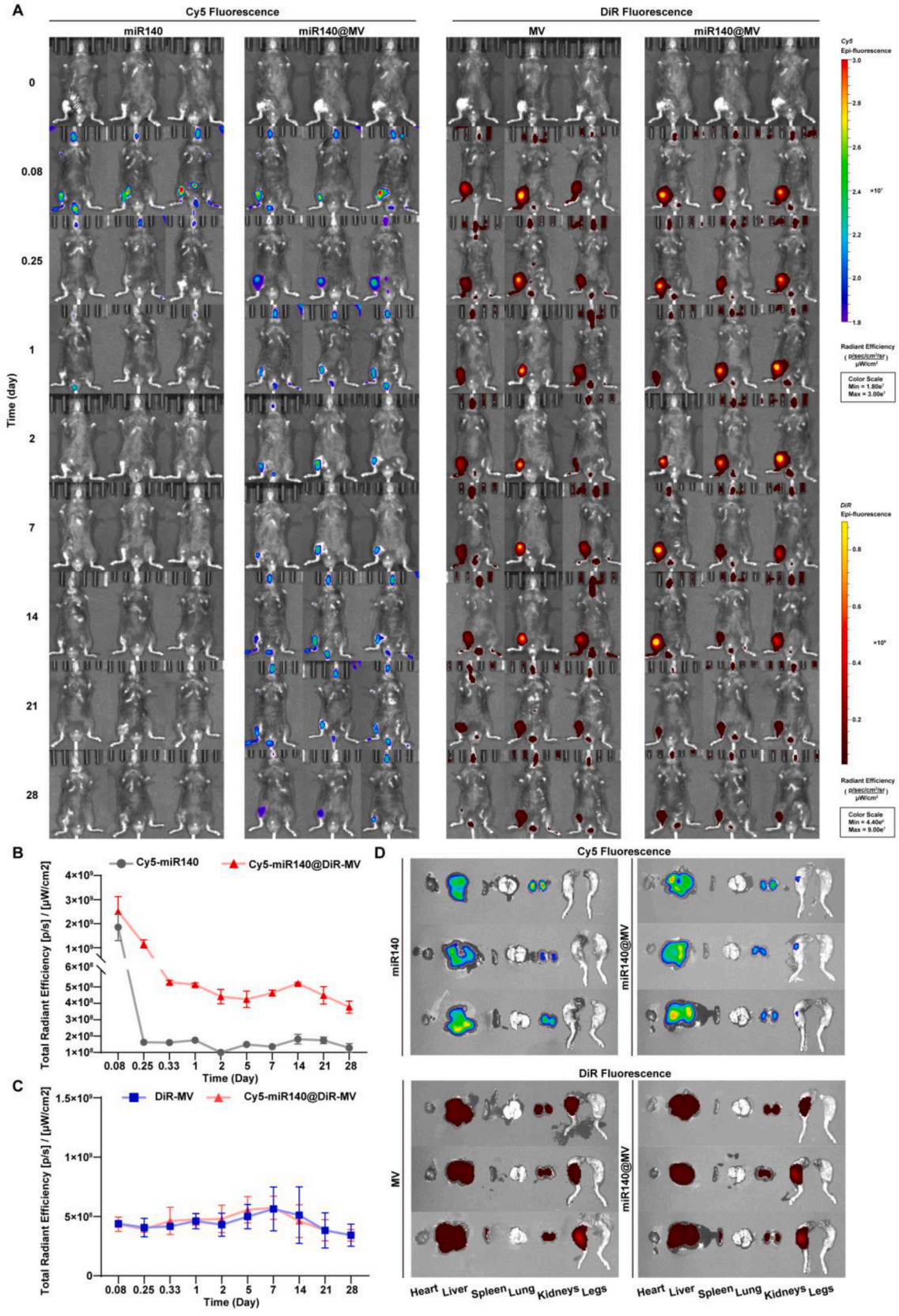

Figure 8 The biodistribution of miR140@MVs for 28 days after administration. (A) The *in vivo* images of Cy5-miR140@DiR-MVs after i.a. injection for different times. Cy5 fluorescence indicates the Cy5-miR140 distribution (Left), and DiR fluorescence indicates the DiR-MVs distribution (Right). (B, C) Region of Interest (ROI) assay of Cy5 (B) and DiR (C) fluorescence intensity in (A). Data are shown as mean ± SEM, $n = 3$. (D) *Ex vivo* images of major organs and legs from DMM mice after 28 days post-injection of Cy5-miR140@DiR-MVs ($n = 3$).

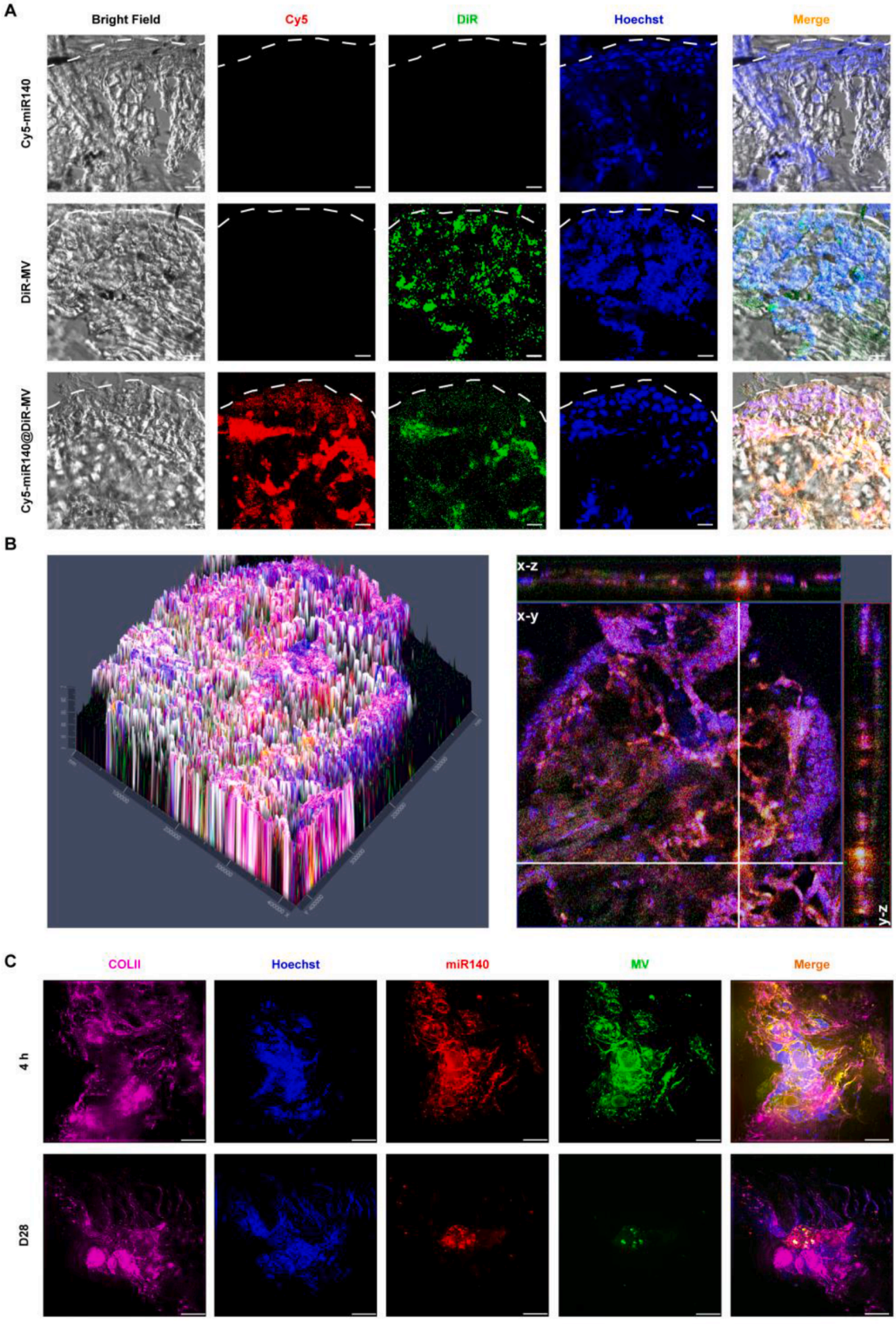

Figure 9 The deep penetration into cartilage and chondrocyte targeting of miR140@MVs *in vivo*. (A) Confocal microscopy images of miR140@MVs distribution in cartilage from DMM mice receiving Cy5-miR140@DiR-MVs for 28 days. miR140 was labeled with Cy5 (Red), MVs were stained by DiR (Green), and nuclei were stained by Hoechst 33342 (Blue). Scale bar: 10 μm. The white dotted line showed the cartilage

In addition, we evaluated the adsorption of MVs on inflammatory factors, such as IL1β and TNFα, which are ascribed to OA progression[53]. ELISA assay showed that MVs and miR140@MVs could neutralize both IL1β and TNFα with saturability of approximately 32 ng of IL1β and 22 ng of TNFα per μg MVs with no significant difference (Supporting Information Fig. S19). These data suggested that MVs as well as miR140@MVs could serve as sponges to adsorb the produced inflammatory cytokines in OA joints, thus alleviating the inflammatory microenvironment.

Collectively, miR140@MVs hold the capabilities of effectively inhibiting the pro-inflammatory effect of macrophages through regulating the phenotypes from M1 towards M2, and neutralizing the existing inflammatory cytokines in the microenvironment, thus remodeling the inflamed OA microenvironment to break the feedback-loop of OA progression.

3.5. *miR140@MVs exhibit obvious anti-inflammation and cartilage protection effects in DMM mice*

To explore whether miR140@MVs could reduce osteoarthritic degeneration and alleviate joint inflammation, an osteoarthritis DMM mouse model was constructed. Mice were randomly divided into 5 groups ($n = 5$ in each group), which were respectively i.a. injected with saline (20 μL), miR140 (700 pmol), MVs (1.5 μg), miRNC@MVs (1.5 μg, corresponding to 700 pmol miRNC), and miR140@MVs (1.5 μg, correspond to 700 pmol miR140) every week for four times (Fig. 6A). The normal and sham-treatment mice (Sham) were used as the healthy controls. To detect the supplementary amount of miR140 in the knee joints, joints of each group were collected at the end of the research. As shown in Fig. 6B, miR140@MVs upregulated nearly 2-fold of miR140 level compared to miR140 alone. Of special note, the miR140 level was also upregulated in the MVs and miRNC@MVs groups, probably owing to the MVs-mediated upregulation of SOX9[33], an upstream gene of miR140, implying a synergistic effect of miR140 and MVs.

Subsequently, we evaluated the therapeutic efficacy by imageological examinations and histological analysis (Fig. 6C). As observed by magnetic resonance imaging (MRI), a widely used examination for clinical OA assessment post-treatments, we found that mice receiving miR140@MVs possessed significantly alleviative inflammation as the weakened brightness indicated by red arrowheads, while other groups maintained severe inflammation, and some groups even showed obviously cartilage defect (yellow arrowheads) or mild bone marrow edema (blue arrowheads) (Fig. 6C). Micro-computed tomography (micro-CT) scan images showed increased osteophyte production of saline, miR140, MVs and miRNC@MVs groups (red dotted circles), indicating excess bone reconstruction. In comparison, miR140@MVs group had a few osteophytes, which were comparable to the normal and sham joints. In addition, the hematoxylin−eosin (H&E) and safranine O-fast green staining of joint sections further confirmed the effective anti-inflammatory and cartilage protection of miR140@MVs with alleviated synovial inflammation as well as smooth and integrity cartilage zone. Whereas other groups exhibited obvious synovial inflammation and a rough irregular cartilage zone due to OA progression. Furthermore, chondrocyte apoptosis was assessed by terminal deoxynucleotidyl transferase dUTP nick end labeling (TUNEL) assay (Fig. 6D and Supporting Information Fig. S20). As expected, OA progression induced more cell apoptosis than that in normal mice (white arrows), while the treatment of miR140@MVs significantly inhibited the cell apoptosis of chondrocytes. Moreover, M2 macrophages made up a larger proportion in miR140@MVs group, while mainly M1 macrophages resided in the synovium of the saline group (Fig. 6D, Supporting Information Figs. S21 and S22), indicating the valid phenotype conversion from M1 to M2 under the treatment of miR140@MVs. Histological scoring that grades the microscopic structure of impaired cartilage and synovial inflammation revealed obvious improvements in cell morphology, matrix staining, cartilage appearance and anti-inflammation of OA knees after miR140@MVs treatment (Fig. 6E). Further, the osteoarthritis research society international (OARSI) score[54] also confirmed the therapeutic effect of miR140@MVs, without significant difference compared with normal and sham groups (Fig. 6F).

To detail the anti-inflammation and cartilage protection of miR140@MVs, qPCR and immunohistochemical analysis were performed. We found that, in contrast with the saline group, miR140@MVs group inhibited 90%, 96%, and 94% expressions of *TNFα, IL6* and *IL1β*, while upregulating 70-fold and 280-fold mRNA levels of *IL10* and *TGFβ*, respectively, suggesting the distinguished anti-inflammatory potential of miR140@MVs (Supporting Information Fig. S23). As for cartilage protection, miR140@MVs group showed the strongest inhibition on both the mRNA and protein levels of *ADAMTS5* and *MMP13* among all the groups, indicating remarkable cartilage protection (Supporting Information Figs. S24 and S25).

We further evaluated the *in vivo* safety of miR140@MVs for the future application of miR140@MVs in OA treatment. The body weights of each group exhibited no obvious variation over time (Supporting Information Fig. S26). The histopathological analysis also suggested no significant tissue toxicity in major organs including heart, liver, spleen, lungs and kidneys (Supporting Information Fig. S27). Moreover, the biochemical indexes of the liver (Alanine transaminase, ALT; aspartate transaminase, AST), and renal (Blood urea nitrogen, BUN; creatinine, CRE; uric acid, UA) in DMM mice treated with miR140@MVs showed no significant changes compared to normal mice (Supporting Information Fig. S28). All these data indicated the well-tolerance of miR140@MVs *in vivo*.

In short, miR140@MVs held potent potential in OA therapy, which could effectively modulate the inflamed microenvironment, inhibit the degradation of cartilage, and promote cartilage repair.

3.6. *miR140@MVs demonstrate a safe and prolonged robust therapeutic effect on DMM mice*

Considering the patient compliance in OA treatment, we wondered whether a single miR140@MVs injection could achieve a satisfactory endpoint of therapy. Thus, we compared the therapeutic effect of miR140@MVs between every week for four consecutive weeks (Multiple miR140@MVs) and only one

boundary. (B) Orthogonal projections illustrating the colocalization of Cy5-miR140 (red) and DiR-MVs (green) in chondrocytes (blue). Left: the 2.5D imaging of the cartilage; Right: the white dotted line indicated the slice for the colocalization analysis, and the orthogonal projection was used to analyze the section of the *x-y* axis and *y-z* axis following the white line. (C) The images of Cy5-miR140@DiR-MVs in cartilage were observed by 3D-SIM. Cartilage was immunostained with COLII (magenta) antibody. Scare bar: 10 μm.

injection for 28 days (Single miR140@MVs). Meanwhile, a single injection of saline served as a negative control (Fig. 7A). We firstly measured the relative level of miR140 in the joints for 28 days (Fig. 7B). Intriguingly, the miR140 level in joints on Day 28 showed no significant difference between single and multiple injections, which gave the chance of miR140@MVs for one-month therapy.

Next, MRI, micro-CT analysis, histological analysis with H&E and safranine O-fast green staining, as well as immunohistochemical staining of CD86 and CD206 were performed. These results showed that single miR140@MVs treatment achieved effective therapeutic effect in parallel to multiple miR140@MVs injections (Fig. 7C and D, Supporting Information Figs. S29−S31), as further confirmed by histological scoring (Fig. 7E). Besides, the qPCR and immunohistochemical staining indicated single miR140@MVs injection exhibited the comparable ability of anti-inflammation (Fig. 7F−J) and cartilage protection (Supporting Information Figs. S32 and S33), compared with multiple miR140@MVs injections. Additionally, a single miR140@MVs injection showed superior biosafety (Supporting Information Fig. S34).

Excitingly, we demonstrated that a single injection of miR140@MVs achieved a safe and effective therapeutic effect for at least 28 days, implying the superior potential of miR140@MVs in clinical applications.

3.7. The mechanism of miR140@MVs in the joints with prolonged therapeutic effect

Having shown the one-month therapeutic effect of miR140@MVs, we wondered what induced the positive results. We firstly evaluated the retention of miR140@MVs *in vivo via* monitoring the double-labeled Cy5-miR140@DiR-MVs after injection into the knee joints of DMM mice for 28 days by using an IVIS spectrum (Fig. 8A). We found that, the Cy5 fluorescence of Cy5-miR140@DiR-MVs decreased at the first 8 h, but plateaued at a relatively high level till 28 days, while that of Cy5-miR140 sharply decreased to an undetected level at 6 h (Fig. 8A and B). On the contrary, the DiR fluorescence in both MVs and Cy5-miR140@DiR-MVs barely decreased (Fig. 8A and C). The *ex vivo* images suggested that miR140@MVs were able to remain in the knee joint for 28 days and were mainly eliminated by the liver and kidneys (Fig. 8D and Supporting Information Fig. S35). Of which, a large amount of MVs could be found in the knee joint, whereas less miR140 remained. The above results suggested that the long retention of miR140 could be attributed to the retention and protection of MVs, thus maintaining the relatively effective miR140 level *in vivo* for 28 days. The prolonged retention of miR140@MVs in OA joints offered the possibility of a one-month therapeutic effect.

Next, we explored the distribution of Cy5-miR140@DiR-MVs in synovium, which acted as the prerequisite for miR140@MVs to regulate synovium macrophages. As exhibited in Supporting Information Fig. S36, Cy5-miR140@DiR-MVs were located in the synovium macrophages labeled by F4/80 at both 4 h and 28 days after injection, wherein miR140 was gradually released from MVs to take effect. Besides, we observed that, Cy5-miR140@DiR-MVs obviously located in the deep region of cartilage, whereas no free Cy5-miR140 could be found in the cartilage frozen section at Day 28 post-injection (Fig. 9A). As chondrocytes are the only cells in cartilage, we further monitored the distribution of Cy5-miR140@DiR-MVs within chondrocytes *via* 2.5D imaging (Fig. 9B) and 3D imaging (Supporting Information Fig. S37, Video 1). The yellow fluorescence of Cy5-miR140@DiR-MVs as well as the separated fluorescence of Cy5-miR140 and DiR-MVs surrounded the chondrocyte nucleus, suggesting the uptake of miR140@MVs by chondrocytes in the deep cartilage and the accompanied miR140 release from MVs. To be clearer, structure illumination microscopy (SIM) was performed to further validate the intracellular distribution of miR140@MVs at 4 h or 28 days post-injection (Fig. 9C). The results showed that most of miR140@MVs around the nuclei of chondrocytes at 4 h after injection, whereas the fluorescence of miR140@MVs weakened at Day 28 owing to the gradual clearance. Of which, Cy5-miR140 dispersed in cytoplasm without overlapping with DiR-MVs, indicating the successful release of miR140 from MVs, as calculated by the Pearson's value decreased nearly 50% (Supporting Information Fig. S38).

Supplementary video related to this article can be found at https://doi.org/10.1016/j.apsb.2025.09.020.

Collectively, the one-month efficacy of miR140@MVs against OA relied on the prolonged retention of miR140@MVs in the knee joint and even in the synovium macrophages and chondrocytes.

4. Discussion

OA has long been considered as a degenerative disease with a high prevalence, which has no convincing drugs till now. The insufficient clinical therapeutic effect includes mainly two facets: (i) single-target drugs are difficult to impede the progress of OA which is a multifactorial disease affecting the whole joints[2] and is aggravated by the metabolic imbalance of senescent chondrocytes and the positive feedback loop of inflamed microenvironment; (ii) current vectors are hard to deliver sufficient drugs, especially nucleic acid drugs to chondrocytes in articular cartilage, owing to the specific structure of articular cartilage and the rapid clearance of joint liquids induced by the movement[2,55]. To address these obstacles, we fabricated a safe and potent miR140@MVs to synergistically remodel the metabolic imbalance of chondrocytes and the inflamed microenvironment, which made a one-month, single-injection treatment regimen for OA therapy possible.

Different from exosomes, MVs are budded from cell membranes, thus retaining most of the functional membrane proteins of the derived cells. In this study, MVs derived from TNFα-stimulated neutrophils retained the membrane proteins such as inflammatory receptors and Anx A1, thus exhibiting superior anti-inflammatory and chondroprotective effects, but avoiding the pro-inflammatory features of neutrophils[56,57]. The non-genetic engineering approach by TNFα stimulation induced the production of MVs with elevated amounts, and enhanced the Anx A1 expression (Fig. 2B and C). Because TNFα stimulation could promote the transport of Anx A1 protein from cytosol to membrane, and augment the budding of MVs from neutrophils[58]. We demonstrated that, the optimized MVs could not only increase the levels of CD206 and *TGFβ* and decrease the levels of *TNFα*, *IL-1β* and *IL-6* of M1-like macrophages (Fig. 5 and Fig. S13), but also elevate the synthesis of COLII by OAC (Fig. 4D and H). These results are in line with the previous report that neutrophil MVs hold the capability of regulating the macrophages[32] and protecting the cartilage[33]. Besides, we found that MVs could adsorb the released inflammatory factors such IL1β and TNFα as the sponge, hence further alleviating the inflamed microenvironment (Fig. S19),

which was similar to the neutrophil membrane that could neutralize the inflammatory cytokines to attenuate inflammation[59]. The combined effect of optimized MVs on remodeling the inflamed microenvironment and promoting COLII synthesis leads to the adjunct therapeutic effect on OA (Fig. 4). Therefore, the strategy of MVs production *via* TNFα-stimulation is facile, effective, short-term, and low-cost, which is favorable for future application.

Another critical role of MVs is autonomously penetrating through the cartilage[33]. Leveraging the merit, the optimized MVs were engaged to deliver miR140 to the chondrocytes distributed in the cartilage in this study. MiR140, a typical miRNA closely associated with the OA progression, has been reported to be significantly declined in OA patients[60,61]. It can synergistically suppress multiple targets to suppress the ECM degradation, promote the survival, proliferation, and cartilage matrix biosynthesis of chondrocytes[23,62], as well as regulate the anti-inflammation effect of macrophages. However, the rapid clearance of miR140 (about 6 h) after i.a. injection led to unsufficient retention to take effect (Fig. 8). Moreover, the difficulty of miR140 into chondrocytes deep distributed in the cartilage matrix further limited their therapeutic effect on OA (Fig. 6). Intriguingly, MVs showed superior effectiveness on improving the miR140 retention in joints till 28 days and promoting the entry of miR140 into chondrocytes and even to the ER to subsequent gene suppression (Fig. 4B, Figs. 7 and 8). More than that, MVs can promote the upregulation of SOX9 which can increase the miR140 level as reported[33], thus achieving a robust efficacy on OA, which is more suitable for clinical application.

Collectively, considering the clinical perspective, we developed a synergized miR140-MVs system to achieve autonomous chondrocyte-targeting and robust therapy effects. It can effectively alleviate inflammation through modulating the macrophages as well as adsorbing the released inflammatory factors to break the feedback-loop of OA progression, and restore the metabolic homeostasis of chondrocytes to arrest and even reverse the cartilage breakdown. The cell-free drug affords the possibility for a one-month, single-injection treatment for OA therapy. Moreover, we propose a modified preparation method of bioactive neutrophil-derived MVs, which can be engaged in other gene therapies for OA or inflammatory joint diseases. Despite promising, the large-scale manufacturing of MVs remains challenging due to the quality control and high-efficiency isolation and purification faced by extracellular vesicles, which restricts the broad application at this stage. Additionally, the long-term effect of miR140@MVs and the critical role of LILRB4 in anti-inflammatory MVs require further exploration.

5. Conclusions

In summary, we developed a synergized miR140@MVs system by leveraging the merits of upgraded anti-inflammatory MVs to achieve autonomous chondrocyte-targeting and prolonged therapy effects. It can effectively alleviate inflammation through modulating the macrophages as well as adsorbing the released inflammatory factors to break the feedback-loop of OA progression, and restore the metabolic homeostasis of chondrocytes to arrest and even reverse the cartilage breakdown. The cell-free drug affords the possibility of a one-month one-injection treatment for OA therapy. Moreover, we propose an upgraded preparation method of bioactive neutrophil-derived MVs, which can be engaged in other gene therapies for OA or inflammatory joint diseases.

Acknowledgments

This work was supported by the National Natural Science Foundation of China (82130102, 92159304, 81930099, and 82073785), the Natural Science Foundation of Jiangsu Province (BK20212011, China), the "Open Competition to Select the Best Candidates" Key Technology Program for Nucleic Acid Drugs of NCTIB (Grant No. NCTIB2022HS01014), "Double First-Class" University Project (CPU2022QZ05, China), National Major Scientific and Technological Special Project for "Significant New Drugs Development" (2019ZX09301163, China), Academic Degree and Postgraduate Education Reform Project of Jiangsu Province (KYCX24_1042, China) and the Open Project of State Key Laboratory of Natural Medicines (China Pharmaceutical University, SKLNMZZ202310). We would like to acknowledge the Public Experimental Platform of China Pharmaceutical University for providing access to the Leica STELLARIS 5 confocal microscope and Multi-SIM imaging system (NanoInsights-Tech Co., Ltd.), and extend sincere gratitude to Ms. Xiaonan Ma for her expert technical assistance and support throughout the experimental process. We also wish to thank Ms. Xiaozhen Yang from the same platform for her valuable technical assistance with the transmission electron microscope (Hitachi HT7700), which contributed significantly to the completion of this study.

Author contributions

Yijun Chen: writing-original draft, project administration, methodology, investigation, formal analysis, data curation, conceptualization. Yongbin Wang: methodology, validation, investigation. Ruonan Yan: validation. Yichen Liu: methodology, validation. Yupeng Dai: investigation. Lingjing Xue: investigation. Caoyun Ju: conceptualization, resources, writing-review & editing, supervision, project administration. Can Zhang: resources, writing-review & editing, supervision, project administration. All authors have approved the final article.

Conflicts of interest

The authors declare no conflicts of interest.

Appendix A. Supporting information

Supporting information to this article can be found online at https://doi.org/10.1016/j.apsb.2025.09.020.

References

1. Hunter DJ, March L, Chew M. Osteoarthritis in 2020 and beyond: a lancet commission. *Lancet* 2020;**396**:1711−2.
2. Martel-Pelletier J, Barr AJ, Cicuttini FM, Conaghan PG, Cooper C, Goldring MB, et al. Osteoarthritis. *Nat Rev Dis Primers* 2016;**2**:16073−91.
3. Tang SA, Zhang C, Oo WM, Fu K, Risberg MA, Bierma-Zeinstra SM, et al. Osteoarthritis. *Nat Rev Dis Primers* 2025;**11**:10−21.
4. Mandl LA. Osteoarthritis year in review 2018: clinical. *Osteoarthr Cartil* 2019;**27**:359−64.
5. Karsdal MA, Michaelis M, Ladel C, Siebuhr AS, Bihlet AR, Andersen JR, et al. Disease-modifying treatments for osteoarthritis

(DMOADs) of the knee and hip: lessons learned from failures and opportunities for the future. *Osteoarthr Cartil* 2016;**24**:2013−21.
6. Rahmati M, Nalesso G, Mobasheri A, Mozafari M. Aging and osteoarthritis: central role of the extracellular matrix. *Ageing Res Rev* 2017;**40**:20−30.
7. Van der Kraan PM, Van den Berg WB. Chondrocyte hypertrophy and osteoarthritis: role in initiation and progression of cartilage degeneration?. *Osteoarthr Cartil* 2012;**20**:223−32.
8. Carlson EL, Karuppagounder V, Pinamont WJ, Yoshioka NK, Ahmad A, Schott EM, et al. Paroxetine-mediated GRK2 inhibition is a disease-modifying treatment for osteoarthritis. *Sci Transl Med* 2021;**13**:8491−505.
9. Sellam J, Berenbaum F. The role of synovitis in pathophysiology and clinical symptoms of osteoarthritis. *Nat Rev Rheumatol* 2010;**6**:625−35.
10. Hwang HS, Kim HA. Chondrocyte apoptosis in the pathogenesis of osteoarthritis. *Int J Mol Sci* 2015;**16**:26035−54.
11. Phillips R. Targeting articular Mmp13 in OA. *Nat Rev Rheumatol* 2021;**17**:645−57.
12. Hu Q, Ecker M. Overview of MMP-13 as a promising target for the treatment of osteoarthritis. *Int J Mol Sci* 2021;**22**:1742−63.
13. Garcia JP, Stein J, Cai Y, Riemers F, Wexselblatt E, Wengel J, et al. Fibrin-hyaluronic acid hydrogel-based delivery of antisense oligonucleotides for ADAMTS5 inhibition in co-delivered and resident joint cells in osteoarthritis. *J Control Release* 2019;**294**:247−58.
14. Glasson SS, Askew R, Sheppard B, Carito B, Blanchet T, Ma HL, et al. Deletion of active ADAMTS5 prevents cartilage degradation in a murine model of osteoarthritis. *Nature* 2005;**434**:644−8.
15. Khan NM, Haseeb A, Ansari MY, Devarapalli P, Haynie S, Haqqi TM. Wogonin, a plant derived small molecule, exerts potent anti-inflammatory and chondroprotective effects through the activation of ROS/ERK/Nrf2 signaling pathways in human osteoarthritis chondrocytes. *Free Radical Bio Med* 2017;**106**:288−301.
16. Chevalier X, Goupille P, Beaulieu AD, Burch FX, Bensen WG, Conrozier T, et al. Intraarticular injection of anakinra in osteoarthritis of the knee: a multicenter, randomized, double-blind, placebo-controlled study. *Arthritis Rheum* 2009;**61**:344−52.
17. Li Y, Wang Y, Chubinskaya S, Schoeberl B, Florine E, Kopesky P, et al. Effects of insulin-like growth factor-1 and dexamethasone on cytokine-challenged cartilage: relevance to post-traumatic osteoarthritis. *Osteoarthr Cartil* 2015;**23**:266−74.
18. Rupaimoole R, Slack FJ. MicroRNA therapeutics: towards a new era for the management of cancer and other diseases. *Nat Rev Drug Discov* 2017;**16**:203−22.
19. Tuddenham L, Wheeler G, Ntounia-Fousara S, Waters J, Hajihosseini MK, Clark I, et al. The cartilage specific microRNA-140 targets histone deacetylase 4 in mouse cells. *FEBS Lett* 2006;**580**:4214−7.
20. Miyaki S, Nakasa T, Otsuki S, Grogan SP, Higashiyama R, Inoue A, et al. MicroRNA-140 is expressed in differentiated human articular chondrocytes and modulates interleukin-1 responses. *Arthritis Rheum* 2009;**60**:2723−30.
21. Liang YJ, Duan L, Xiong JY, Zhu WM, Liu QS, Wang DM, et al. E2 regulates MMP-13 *via* targeting miR-140 in IL-1β-induced extracellular matrix degradation in human chondrocytes. *Arthritis Res Ther* 2016;**18**:105.
22. Inui M, Mokuda S, Sato T, Tamano M, Takada S, Asahara H. Dissecting the roles of miR-140 and its host gene. *Nat Cell Biol* 2018;**20**:516−8.
23. Wang Z, Hu JL, Pan Y, Shan YJ, Jiang LQ, Qi X, et al. miR-140-5p/miR-149 affects chondrocyte proliferation, apoptosis, and autophagy by targeting FUT1 in osteoarthritis. *Inflammation* 2018;**41**:959−71.
24. Ghafouri-Fard S, Bahroudi Z, Shoorei H, Abak A, Ahin M, Taheri M. microRNA-140: a miRNA with diverse roles in human diseases. *Biomed Pharmacother* 2021;**135**:111256−71.
25. Evans CH, Kraus VB, Setton LA. Progress in intra-articular therapy. *Nat Rev Rheumatol* 2014;**10**:11−22.
26. Zhao TY, Li X, Li H, Deng HY, Li JW, Yang Z, et al. Advancing drug delivery to articular cartilage: from single to multiple strategies. *Acta Pharm Sin B* 2023;**13**:4127−48.
27. Bajpayee AG, Grodzinsky AJ. Cartilage-targeting drug delivery: can electrostatic interactions help?. *Nat Rev Rheumatol* 2017;**13**:183−93.
28. Hu Q, Chen Q, Yan XY, Ding BM, Chen DW, Cheng LF. Chondrocyte affinity peptide modified PAMAM conjugate as a nanoplatform for targeting and retention in cartilage. *Nanomedicine* 2018;**13**:749−67.
29. Li BX, Cui L, Kong KY, Pang YC, Chen Y, Zhang SN, et al. LNP-mRNA delivers TNF-α antibody to deep cartilage and protects against osteoarthritis. *Chem Eng J* 2024;**500**:156723−43.
30. Geiger BC, Wang S, Padera Jr RF, Grodzinsky AJ, Hammond PT. Cartilage-penetrating nanocarriers improve delivery and efficacy of growth factor treatment of osteoarthritis. *Sci Transl Med* 2018;**10**:8800−12.
31. Bajpayee AG, De la Vega RE, Scheu M, Varady NH, Yannatos IA, Brown LA, et al. Sustained intra-cartilage delivery of low dose dexamethasone using a cationic carrier for treatment of post traumatic osteoarthritis. *Eur Cell Mater* 2017;**34**:341−64.
32. Rhys HI, Dell'Accio F, Pitzalis C, Moore A, Norling LV, Perretti M. Neutrophil microvesicles from healthy control and rheumatoid arthritis patients prevent the inflammatory activation of macrophages. *EBioMedicine* 2018;**29**:60−9.
33. Headland Sarah E, Jones Hefin R, Norling Lucy V, Kim A, Souza Patricia R, Corsiero E, et al. Neutrophil-derived microvesicles enter cartilage and protect the joint in inflammatory arthritis. *Sci Transl Med* 2015;**7**:190−202.
34. Zhan D, Cross A, Wright HL, Moots RJ, Edwards SW, Honsawek S. Internalization of neutrophil-derived microvesicles modulates TNFα-Stimulated proinflammatory cytokine production in human fibroblast-like synoviocytes. *Int J Mol Sci* 2021;**22**:7409−28.
35. Gomez I, Ward B, Souilhol C, Recarti C, Ariaans M, Johnston J, et al. Neutrophil microvesicles drive atherosclerosis by delivering-to atheroprone endothelium. *Nat Commun* 2020;**11**:214−32.
36. Gosset M, Berenbaum F, Thirion S, Jacques C. Primary culture and phenotyping of murine chondrocytes. *Nat Protoc* 2008;**3**:1253−60.
37. Xue JW, Zhao ZK, Zhang L, Xue LJ, Shen SY, Wen YJ, et al. Neutrophil-mediated anticancer drug delivery for suppression of postoperative malignant glioma recurrence. *Nat Nanotechnol* 2017;**12**:692−700.
38. Du JJ, Wang C, Chen YJ, Zhong LY, Liu XW, Xue LJ, et al. Targeted downregulation of HIF-1α for restraining circulating tumor microemboli mediated metastasis. *J Control Release* 2022;**343**:457−68.
39. Li YY, Hu QF, Li WS, Liu SJ, Li KM, Li XY, et al. Simultaneous blockage of contextual TGF-β by cyto-pharmaceuticals to suppress breast cancer metastasis. *J Control Release* 2021;**336**:40−53.
40. Zhao LW, Gu CY, Gan Y, Shao LL, Chen HW, Zhu HY. Exosome-mediated siRNA delivery to suppress postoperative breast cancer metastasis. *J Control Release* 2020;**318**:1−15.
41. Zhao YM, Zheng YL, Zhu Y, Zhang Y, Zhu HY, Liu TQ. M1 Macrophage-derived exosomes loaded with gemcitabine and deferasirox against chemoresistant pancreatic cancer. *Pharmaceutics* 2021;**13**:1493.
42. Glasson SS, Blanchet TJ, Morris EA. The surgical destabilization of the medial meniscus (DMM) model of osteoarthritis in the 129/SvEv mouse. *Osteoarthr Cartil* 2007;**15**:1061−9.
43. Chen YJ, Li KM, Jiao MY, Huang YS, Zhang ZH, Xue LJ, et al. Reprogrammed siTNFα/neutrophil cytopharmaceuticals targeting inflamed joints for rheumatoid arthritis therapy. *Acta Pharm Sin B* 2023;**13**:787−803.
44. Jeppesen DK, Fenix AM, Franklin JL, Higginbotham JN, Zhang Q, Zimmerman LJ, et al. Reassessment of exosome composition. *Cell* 2019;**177**:428−45.
45. Tian Y, Zhang F, Qiu YF, Wang S, Li F, Zhao JW, et al. Reduction of choroidal neovascularization *via* cleavable VEGF antibodies conjugated to exosomes derived from regulatory T cells. *Nat Biomed Eng* 2021;**5**:968−82.
46. Lavin Y, Mortha A, Rahman A, Merad M. Regulation of macrophage development and function in peripheral tissues. *Nat Rev Immunol* 2015;**15**:731−44.

47. Reid DW, Nicchitta CV. Diversity and selectivity in mRNA translation on the endoplasmic reticulum. *Nat Rev Mol Cell Biol* 2015;**16**: 221−31.
48. Heusermann W, Hean J, Trojer D, Steib E, von Bueren S, Graff-Meyer A, et al. Exosomes surf on filopodia to enter cells at endocytic hot spots, traffic within endosomes, and are targeted to the ER. *J Cell Biol* 2016;**213**:173−84.
49. Zhang R, Ma J, Yao J. Molecular mechanisms of the cartilage-specific microRNA-140 in osteoarthritis. *Inflamm Res* 2013;**62**: 871−7.
50. Sanchez-Lopez E, Coras R, Torres A, Lane NE, Guma M. Synovial inflammation in osteoarthritis progression. *Nat Rev Rheumatol* 2022; **18**:258−75.
51. Zhang H, Cai D, Bai X. Macrophages regulate the progression of osteoarthritis. *Osteoarthr Cartil* 2020;**28**:555−61.
52. Sun ZY, Liu QQ, Lv ZY, Li JW, Xu XQ, Sun H, et al. Targeting macrophagic SHP2 for ameliorating osteoarthritis TLR signaling. *Acta Pharm Sin B* 2022;**12**:3073−84.
53. Kapoor M, Martel-Pelletier J, Lajeunesse D, Pelletier JP, Fahmi H. Role of proinflammatory cytokines in the pathophysiology of osteoarthritis. *Nat Rev Rheumatol* 2011;**7**:33−42.
54. Zhu JJ, Yang SH, Qi YD, Gong Z, Zhang HT, Liang KY, et al. Stem cell-homing hydrogel-based miR-29b-5p delivery promotes cartilage regeneration by suppressing senescence in an osteoarthritis rat model. *Sci Adv* 2022;**8**:11−27.
55. Wang XJ, Han XJ, Li CZ, Chen Z, Huang H, Chen JD, et al. 2D materials for bone therapy. *Adv Drug Deliv Rev* 2021;**178**: 113970−92.
56. Kolaczkowska E, Kubes P. Neutrophil recruitment and function in health and inflammation. *Nat Rev Immunol* 2013;**13**:159−75.
57. Khandpur R, Carmona-Rivera C, Vivekanandan-Giri A, Gizinski A, Yalavarthi S, Knight JS, et al. NETs are a source of citrullinated autoantigens and stimulate inflammatory responses in rheumatoid arthritis. *Sci Transl Med* 2013;**5**:178−99.
58. Perretti M, Solito E. Annexin 1 and neutrophil apoptosis. *Biochem Soc Trans* 2004;**32**:507−10.
59. Zhang QZ, Dehaini D, Zhang Y, Zhou JL, Chen XY, Zhang LF, et al. Neutrophil membrane-coated nanoparticles inhibit synovial inflammation and alleviate joint damage in inflammatory arthritis. *Nat Nanotechnol* 2018;**13**:1182−90.
60. Wang PP, Zhou Y, Richards AM. Effective tools for RNA-derived therapeutics: siRNA interference or miRNA mimicry. *Theranostics* 2021;**11**:8771−96.
61. Zhang Y, Li SJ, Jin PS, Shang T, Sun RZ, Lu LY, et al. Dual functions of microRNA-17 in maintaining cartilage homeostasis and protection against osteoarthritis. *Nat Commun* 2022;**13**:2447−58.
62. Duan L, Liang YJ, Xu X, Xiao Y, Wang DP. Recent progress on the role of miR-140 in cartilage matrix remodelling and its implications for osteoarthritis treatment. *Arthritis Res Ther* 2020;**22**: 194−203.